CEP78 functions downstream of CEP350 to control biogenesis of primary cilia by negatively regulating CP110 levels

André Brás Gonçalves[1], Beinta Biskopstø Joensen[1,5], Sarah Kirstine Hasselbalch[1,5], Pernille Martens[1], Signe Krogh Ohlsen[2], Mathieu Quinodoz[3,3.1,3.2], Konstantinos Nikopoulos[3], Magnus Per Damsø Jeppesen[1], Catja Weiss[1], Søren Tvorup Christensen[1], Sebastian Patzke[4], Carlo Rivolta[3,3.1,3.2], Jens S. Andersen[2], Pietro Farinelli[1*] and Lotte Bang Pedersen[1*]

[1]Department of Biology, Section for Cell Biology and Physiology, University of Copenhagen, Universitetsparken 13, DK-2100 Copenhagen Ø, Denmark

[2]Department of Biochemistry and Molecular Biology, University of Southern Denmark, Campusvej 55, 5230 Odense M, Denmark

[3]Institute of Molecular and Clinical Ophthalmology Basel (IOB), Basel, Switzerland

[3.1]Department of Ophthalmology, University of Basel, Basel, Switzerland

[3.2]Department of Genetics and Genome Biology, University of Leicester, Leicester, United Kingdom

[4]Department of Radiation Biology, Institute for Cancer Research, Norwegian Radium Hospital, Oslo University Hospital, Oslo, Norway

[5]These authors contributed equally to this study

[*]For correspondance: Pietro.Farinelli@twelve.bio (PF); lbpedersen@bio.ku.dk (LBP)

Abstract

CEP78 is a centrosomal protein implicated in ciliogenesis and ciliary length control, and mutations in the *CEP78* gene cause retinal cone-rod dystrophy associated with hearing loss. However, the mechanism by which CEP78 affects cilia formation is unknown. Based on a recently-discovered disease-causing *CEP78* p.L150S mutation, we identified the disease-relevant interactome of CEP78. We confirmed that CEP78 interacts with the EDD1-DYRK2-DDB1^{VPRBP} E3 ubiquitin ligase complex, which is involved in CP110 ubiquitination and degradation, and identified a novel interaction between CEP78 and CEP350 that is weakened by the CEP78^{L150S} mutation. We show that CEP350 promotes centrosomal recruitment and stability of CEP78, which in turn leads to centrosomal recruitment of EDD1. Consistently, cells lacking CEP78 display significantly increased cellular and centrosomal levels of CP110, and depletion of CP110 in CEP78-deficient cells restored ciliation frequency to normal. We propose that CEP78 functions downstream of CEP350 to promote ciliogenesis by negatively regulating CP110 levels via an EDD1-dependent mechanism.

Introduction

Primary cilia are antenna-like sensory organelles that play pivotal roles in coordinating various signaling pathways important for human development and tissue homeostasis [1]. They comprise a microtubule-based axoneme core, which extends directly from the mother centriole-derived basal body and is surrounded by a bilayer membrane enriched for specific receptors, ion channels and lipids that endow the organelle with unique signaling properties [2]. Not surprisingly, mutations in genes that affect assembly, structure or function of primary cilia are causative for a growing number of pleiotropic diseases and syndromes called ciliopathies, which include cone-rod dystrophy in the retina and hearing loss (CRDHL; MIM# 617236) amongst others [3]. Ciliopathy genes include those coding for components of the centrosome, which contains the daughter and mother centriole and gives rise to the ciliary basal body. The mother centriole is distinguished from the daughter centriole by distal and subdistal appendages, which play critical roles in vesicle docking at the onset of ciliogenesis and in microtubule anchoring, respectively. In addition, the centrosome contains pericentriolar material and is associated with centriolar satellites that affect cilia biogenesis and function in various ways [4].

Assembly of primary cilia is a complex, multistep process that is tightly coordinated with the cell cycle. In actively-proliferating cells, centriolar coiled coil protein 110 (CP110; also known as CCP110) and centrosomal protein of 97 kDa (CEP97) cap the distal ends of both mother and daughter centrioles and suppress ciliogenesis. Furthermore, overexpression of CP110 in growth-arrested cells prevents ciliogenesis [5]. CP110 also regulates centriole duplication and length control during S phase and interacts with key regulators of centriole duplication, including PLK4 [6-9]. As cells enter G1/G0, ciliogenesis begins with recruitment of pre-ciliary vesicles to the distal end of the mother centriole. The vesicles subsequently fuse to form a larger ciliary vesicle underneath which the ciliary transition zone and axoneme are assembled. The axoneme is further extended by intraflagellar transport (IFT), and the ciliary vesicle expands and matures to form the ciliary membrane and a surrounding sheath that fuses with the plasma membrane upon completion of ciliogenesis [10-12].

Initiation of transition zone formation and axoneme extension during early stages of ciliogenesis requires removal of the CEP97-CP110 complex from the distal end of the mother centriole [5]. This process relies on M-Phase Phosphoprotein 9 (MPP9), which interacts directly with CEP97 and cooperates with kinesin KIF24 to recruit the CEP97-CP110 complex to the distal centriole end [13, 14]. During ciliogenesis, phosphorylation of MPP9 by Tau tubulin kinase 2 (TTBK2) leads to degradation of MPP9 by the ubiquitin proteasome system (UPS), which results in destabilization of

78 the CEP97-CP110 complex causing its removal from the distal end of the mother centriole [14].
79 TTBK2 is recruited to the mother centriole distal appendages by CEP164 [15, 16] where it also
80 phosphorylates CEP83 to promote CP110 removal [17]. Consequently, depletion of CEP164,
81 TTBK2, CEP83 or other centriole distal appendage proteins that regulate their localization and/or
82 function impairs ciliogenesis [18-23]. Mother centriole recruitment of TTBK2 and removal of the
83 distal CEP97-CP110 cap additionally requires the subdistal CEP350-FOP-CEP19 complex, which
84 furthermore interacts with RABL2 and IFT-B complex components to promote their axonemal en-
85 try [24-26].
86 Despite recent advances, the precise mechanisms by which CP110 regulates ciliogenesis and
87 is removed from the mother centriole at the onset of ciliogenesis remain incompletely understood.
88 For example, a recent study implicated the homologous to the E6AP carboxyl terminus (HECT)
89 type EDD1-DYRK2-DDB1^{VPRBP} E3 ligase complex in ubiquitination and degradation of CP110 via
90 a mechanism involving direct interaction of viral protein R binding protein (VPRBP; also known as
91 DCAF1) and centrosomal protein of 78 kDa (CEP78) [27]. Specifically, the authors reported that
92 CEP78 suppresses CP110 ubiquitination by EDD1 (also known as UBR5 and EDD) and it was pro-
93 posed that CP110 is phosphorylated by DYRK2 and thereby recognized and brought close to EDD1
94 by VPRBP. EDD1 then transfers ubiquitin to CP110 leading to its degradation. When CEP78 binds
95 VPRBP it induces a conformational change in the complex thereby preventing CP110 ubiquitina-
96 tion. Further, they demonstrated that depletion of CEP78 promoted centriole elongation, whereas
97 *CEP78* over-expression inhibited primary cilia formation in hTERT-immortalized retinal pigment
98 epithelial (RPE1) cells [27]. On the other hand, knockout (KO) of *Dyrk2* in the mouse was reported
99 to result in elongation of primary cilia, but centrosomal CP110 levels appeared unaffected in *Dyrk2*
100 mouse KO cells [28]. Therefore, it remains uncertain how CEP78 and the EDD1-DYRK2-
101 DDB1^{VPRBP} complex affect CP110 homeostasis to control ciliogenesis.
102 *CEP78* is composed of 16 exons and encodes a protein comprising 722 amino acids that
103 possesses five consecutive leucine rich repeats (LRR) at the N-terminus, and a coiled-coil (CC) do-
104 main at the C-terminus [29, 30]. Four independent studies have reported eight different mutations in
105 *CEP78* in patients with CRDHL [29-32], whereas one study identified a homozygous *CEP78*-trun-
106 cating variant in a family with non-syndromic retinitis pigmentosa (MIM# 268003; [33]), another
107 form of retinal degeneration. Of these studies, two have investigated the functional consequences of
108 human *CEP78* mutations at the cellular level. In one study, whole-exome sequencing (WES) identi-
109 fied biallelic mutations in *CEP78* in two unrelated families from Greece and Sweden, respectively

110 [29]. The Greek subject had a homozygous base substitution at the splice donor site in intron 3 of
111 *CEP78* (NM_032171.2:c.499+1G>T). Two subjects from a Swedish family carried heterozygous
112 mutations, one base substitution in intron 3 (NM_032171.2:c.499+5G>A) and a single nucleotide
113 deletion in exon 5 (NM_032171.2:c.633del; p.Trp212GlyfsTer18) causing a frameshift. These
114 *CEP78* mutations lead to exon skipping and premature stop codons accompanied by almost unde-
115 tectable levels of CEP78 protein in human skin fibroblasts (HSFs) of affected individuals. Further-
116 more, it was found that HSFs from these patients have significantly longer primary cilia as com-
117 pared to control cells [29]. More recently, a missense mutation in *CEP78*
118 (NM_032171.2:c.449T>C; p.Leu150Ser) was identified in three unrelated families from Belgium
119 and Germany diagnosed with CRDHL [30]. In the two Belgian families, affected individuals were
120 homozygous for the p.Leu150Ser variant, whereas affected individuals from the German family dis-
121 played compound heterozygosity for this variant and a novel splice site variant,
122 NM_032171.2:c.1462-1G>T. In all cases, HSFs from patients harboring the p.Leu150Ser mutation
123 (hereafter: L150S) displayed decreased cellular levels of CEP78 and significantly elongated cilia
124 compared to control HSFs [30], as seen in patient-derived HSFs with CEP78 truncating mutations
125 [29]. In addition, other ciliopathy features were reported in some of the affected individuals with the
126 $CEP78^{L150S}$ mutation, including obesity, respiratory problems, diabetes 2 and infertility [30]. In
127 summary, available data derived from human patients indicates that depletion of CEP78 leads to
128 elongation of primary cilia at the cellular level, which manifests in ciliopathy phenotypes at the or-
129 ganism level. However, the mechanism by which CEP78 regulates ciliary length is not known.
130 In addition to the patient studies described above, some studies have addressed CEP78 func-
131 tion in different cell culture models. First, a study showed that siRNA-mediated depletion of CEP78
132 in RPE1 cells reduces the frequency of cells forming primary cilia, possibly due to centriolar an-
133 choring defects, but the length of the residual cilia was not assessed. Similarly, depletion of CEP78
134 in *Planarians* was shown to impair motile cilia formation due to defective docking of centrioles to
135 the cell surface [34]. Another study identified CEP78 interaction with PLK4 and implicated CEP78
136 in PLK4-mediated centriole over duplication, whereas possible roles for CEP78 in relation to cilia
137 were not addressed [35]. Finally, as mentioned above, a study reported that CEP78 directly interacts
138 with VPRBP of the EDD1-DYRK2-$DDB1^{VPRBP}$ E3 ligase complex to suppress CP110 ubiquitina-
139 tion and thereby stabilize it [27]. How such CEP78-mediated stabilization of CP110 might lead to
140 the long cilia phenotype observed in patient fibroblasts lacking CEP78 [29, 30] and/or the reduced
141 ciliation frequencies seen in CEP78-depleted *Planarians* and RPE1 cells [34] is unclear.

142 Here were show that in RPE1 cells and patient-derived HSFs loss of CEP78 leads to reduced
143 ciliation frequency as well as increased length of the cilia that do form. By taking advantage of the
144 recently identified disease-causing CEP78^{L150S} mutation [30], we used a quantitative mass spec-
145 trometry-based approach to identify a disease-relevant interactome of CEP78. We confirmed that
146 CEP78 interacts with the EDD1-DYRK2-DDB1^{VPRBP} complex implicated in CP110 ubiquitination
147 and degradation [27], and furthermore identified a novel interaction between CEP78 and the N-ter-
148 minal region of CEP350. The interaction of CEP78 with both VPRBP and CEP350, as well as cen-
149 trosomal recruitment of CEP78, are dramatically reduced by the CEP78^{L150S} mutation. Lack of cen-
150 trosomal recruitment of CEP78^{L150S} is likely due to impaired interaction with CEP350 since centro-
151 somal and cellular levels of CEP78 were significantly decreased in *CEP350* KO cells. Conversely,
152 cells lacking CEP78 displayed significantly decreased centrosomal levels of EDD1 and unaltered or
153 slightly increased centrosomal levels of CEP350. In addition, CEP78-deficient cells showed signifi-
154 cantly increased cellular and centrosomal levels of CP110, presumably owing to the reduced centro-
155 somal levels of EDD1 observed in these cells, and depletion of CP110 in CEP78-deficient cells re-
156 stored ciliation frequency to normal. Collectively our results suggest that CEP78 functions down-
157 stream of CEP350 to promote cilia biogenesis by negatively regulating CP110 levels via an EDD1-
158 dependent mechanism.
159

160 ## Results

161 **Depletion of CEP78 leads to fewer and longer primary cilia in cultured cells**

162 Previous studies showed that patient-derived fibroblasts lacking CEP78 display significantly elon-
163 gated primary cilia compared to control cells [29, 30] whereas depletion of CEP78 in *Planarians*
164 and RPE1 cells was shown to significantly reduce cilia numbers [34]. To reconcile these seemingly
165 contradictory findings we analyzed cilia numbers and length in serum-deprived wild type (WT) and
166 *CEP78* KO RPE1 cells [30] by immunofluorescence microscopy (IFM) with antibodies against cili-
167 ary (ARL13B) and centrosomal (CEP350) markers. We found that the frequency of ciliated cells is
168 significantly reduced in *CEP78* KO cells compared to WT cells (Figure 1A, B) whereas the length
169 of the remaining cilia is significantly increased in the *CEP78* KO cells (Figure 1A, C). Similar re-
170 sults were obtained using previously described patient-derived *CEP78*-deficient or control HSFs
171 (Figure 1D-F) [29, 30]. The low ciliation frequencies of serum-deprived *CEP78* mutant cells were
172 not secondary to cell cycle defects, as judged by western blot analysis with antibody against reti-
173 noblastoma protein phosphorylated at S807/811 (P-Rb; Figure 1G-L). However, in serum-fed cells,

174 P-Rb levels were significantly higher in *CEP78* mutant cells compared to controls (Figure 1G-L),
175 indicating that mutant cells may progress slower through S-phase [36]. This is in line with previous
176 reports indicating that CEP78 protein levels are upregulated in late S-G2 phase suggesting a role for
177 CEP78 at this cell cycle stage, e.g. during centriole duplication [27, 35]. We conclude that CEP78
178 deficient RPE1 and HSF cells display reduced ciliation frequencies as well as increased length of
179 remaining cilia, thus reconciling previous observations [29, 30, 34].
180
181 **Analysis of RPE1 WT and *CEP78* KO cells expressing FLAG-CEP78 and FLAG-CEP78^{L150S}**
182 To confirm the above results, we performed a rescue experiment by transiently expressing FLAG-
183 CEP78 in WT and *CEP78* KO RPE1 cells followed by serum-deprivation and IFM analysis using
184 FLAG and ARL13B antibodies. In parallel, we performed similar experiments with FLAG-
185 CEP78^{L150S}. We first analyzed the localization and expression levels of the two FLAG fusions in
186 serum-deprived RPE1 cells. The FLAG-CEP78 fusion protein localized to both centrioles at the
187 base of cilia as expected [27, 29, 35], whereas centriolar localization of FLAG-CEP78^{L150S} was se-
188 verely compromised although not completely abolished (Figure 2A, B). The latter result is in line
189 with previous reports showing that the LRR region in the N-terminus of CEP78, which encom-
190 passes residue L150, is important for its localization to centrioles [27, 35]. Both FLAG fusions were
191 expressed at similar levels in the cells (Figure 2-figure supplement 1A, B); this was somewhat sur-
192 prising given that endogenous CEP78^{L150S} is largely undetectable by western blot analysis of pa-
193 tient-derived HSFs suggesting its stability is compromised [30]. Therefore, we tested if the L150S
194 mutation might affect binding of the CEP78 antibody used in [30] to CEP78. However, FLAG im-
195 munoprecipitation (IP) and western blot analysis of 293T cells expressing FLAG-CEP78 or FLAG-
196 CEP78^{L150S} indicated that the CEP78 antibody binds equally well to WT CEP78 and the CEP78^{L150S}
197 mutant protein. This analysis also revealed that endogenous CEP78 co-IPs with FLAG-CEP78 indi-
198 cating that CEP78 can form homodimers/oligomers (Figure 2-figure supplement 2). These results
199 indicate that the L150S mutation compromises the recruitment of CEP78 to the centrosome, but not
200 its short-term stability, at least in RPE1 cells. We cannot rule out that the N-terminal FLAG tag may
201 stabilize FLAG-CEP78^{L150S} and prevent it from being degraded.
202 Next, we tested if FLAG-CEP78 or FLAG-CEP78^{L150S} could rescue the ciliary phenotypes
203 of *CEP78* KO cells. In WT cells, transient expression of FLAG-CEP78 lead to reduced ciliation fre-
204 quency compared to non-transfected cells, in agreement with a previous study [27], although this
205 result was not statistically significant (Figure 2C). Surprisingly, ciliated WT cells expressing

206 FLAG-CEP78 were significantly elongated compared to non-transfected controls, similar to un-
207 transfected *CEP78* KO cells (Figure 1D). In contrast, expression of FLAG-CEP78 in the *CEP78*
208 KO cells rescued the ciliary length phenotype of these cells (Figure 1D), indicating that precise con-
209 trol of cellular/centrosomal levels of CEP78 is needed for appropriate ciliary length control, with
210 too much or too little CEP78 causing ciliary lengthening. Since transient expression of FLAG-
211 CEP78 in the *CEP78* KO cells caused ciliary shortening (Figure 1D) it was not possible to assess
212 whether this fusion protein could also rescue the reduced ciliation frequency phenotype of these
213 cells. While the *CEP78* KO cells expressing FLAG-CEP78 still displayed significantly fewer cilia
214 than WT cells (Figure 1C), we cannot exclude that the transfected *CEP78* KO cells initially had
215 more cilia, which progressively became shorter and eventually disappeared during the course of the
216 experiment (see also below and Figure 8 for rescue of the ciliation frequency phenotype of the
217 *CEP78* KO cells). Finally, we obtained essentially identical results upon expression of FLAG-
218 CEP78^{L150S} in both WT and *CEP78* KO cells (Figure 2C, D) indicating that despite its reduced lo-
219 calization to centrioles (Figure 1A, B), this mutant protein is still able to influence ciliary length in a
220 manner paralleling WT FLAG-CEP78.
221 Taken together, our results indicate that 1) loss of CEP78 causes reduced ciliation frequency
222 as well as increased length of remaining cilia in both RPE1 and HSF cells; 2) overexpression of
223 CEP78 similarly leads to fewer but longer cilia; and 3) the L150S mutation compromises localiza-
224 tion of CEP78 to centrioles, but not its short-term stability and ability to influence ciliary length.
225
226 **CEP78 interacts with the EDD1-DYRK2-DDB1^{VPRBP} complex and CEP350**
227 To explore how CEP78 is recruited to centrioles to regulate ciliary frequency and length we first
228 used Stable Isotope Labeling by Amino acids in Cell culture (SILAC)-based quantitative mass spec-
229 trometry (MS) to identify the differential interactomes of FLAG-CEP78 and FLAG-CEP78^{L150S} ex-
230 pressed in 293T cells (see Materials and methods for details). We identified interaction between
231 CEP78 and several components of the EDD1-DYRK2-DDB1^{VPRBP} complex (Figure 3A), in agree-
232 ment with previous work showing direct binding of CEP78 to VPRBP within this complex [27]. In-
233 terestingly, the MS results indicated that the CEP78^{L150S} mutation dramatically reduces this interac-
234 tion (Figure 3A), which we confirmed by IP and western blot analysis of 293T cells co-expressing
235 Myc-VPRBP and FLAG-CEP78 or FLAG-CEP78^{L150S} (Figure 3B). In addition, our interactome
236 analysis identified CEP350 as potential novel CEP78 binding partner (Figure 3A). Using IP and
237 western blot analysis in 293T cells co-expressing FLAG-CEP78 or FLAG-CEP78^{L150S} with a Myc-

238 tagged N-terminal or C-terminal CEP350 truncation we found that CEP78 binds to the N-terminal
239 region of CEP350 (residues 1-983; Figure 3C, E); reciprocal co-IP with Myc-tagged CEP350 con-
240 structs confirmed this result (Figure 3-figure supplement 1). Furthermore, we found that the interac-
241 tion between CEP78 and CEP350 N-terminus is reduced by the CEP78^{L150S} mutation (Figure 3C).
242 Using a similar approach, we could not detect interaction between CEP78 and endogenous FOP
243 (Figure 3C), whereas under similar conditions endogenous FOP was readily co-IPed with the C-ter-
244 minus of CEP350 (Figure 3-figure supplement 1), in agreement with a previous report [37]. We also
245 mapped the CEP350 interaction site in CEP78 and found that CEP350 primarily binds to the C-ter-
246 minal region of CEP78 comprising residues 395-722 (Figure 3D, E), although a weak interaction
247 with a fragment comprising the entire LRR region (residues 2-403) was also observed. In contrast,
248 truncation of the latter fragment into two smaller fragments abolished binding to the CEP350 N-ter-
249 minus (Figure 3D, E). Binding of CEP78 to VPRBP similarly requires the entire LRR region of
250 CEP78 [27] and we therefore wondered whether interaction between CEP350 and CEP78 might be
251 mediated by VPRBP. However, IP experiments and western blot analysis failed to reveal physical
252 interaction between VPRBP and CEP350 N-terminus (Figure 3, figure supplement 1). We conclude
253 that CEP78 binds independently to VPRBP and the N-terminus of CEP350 and that both of these
254 interactions are reduced by the CEP78^{L150S} mutation.
255
256 **CEP350 regulates the stability and centrosomal recruitment of CEP78**
257 In non-ciliated HeLa and U2OS cells CEP78 localizes to both centrioles during all phases of the
258 cell cycle and appears to concentrate at the centriole wall [35]. In ciliated RPE1 cells CEP78 was
259 shown to localize to the distal end of both centrioles, with a preference for the mother centriole/ba-
260 sal body [27]. Similarly, CEP350 was reported to localize to the distal end of the mother centri-
261 ole/basal body, near the subdistal appendages, in ciliated RPE1 cells [24, 26, 38]. In agreement with
262 these reports and with our interactome and IP results (Figure 3), 3D Structured Illumination Micros-
263 copy (SIM) showed partial co-localization of CEP78 with CEP350 at the distal end of the basal
264 body of ciliated RPE1 cells, beneath the distal appendage marker CEP164 (Figure 4A). Further-
265 more, using a previously characterized RPE1 *CEP350* KO cell line [24], we found that depletion of
266 CEP350 not only reduces localization of CEP78 to the centrosome, but also its total cellular level
267 (Figure 4B-G). Similarly, we found significantly reduced levels of CEP78 in *FOP* KO cells (Figure
268 4 B, C), in line with the decreased centrosomal levels of CEP350 observed in these cells [24]. These

269 results indicate that CEP350 promotes the recruitment of CEP78 to the mother centriole/basal body
270 as well as its overall stability.
271
272 **CEP78 mutant cells display reduced centrosomal levels of EDD1**
273 Next, we asked if CEP78 might affect the centrosomal recruitment of components of the EDD1-
274 DYRK2-DDB1^{VPRBP} complex and/or CEP350, and analyzed the cellular or centrosomal levels of
275 relevant complex components in RPE1 WT and *CEP78* KO cells. The results showed that serum-
276 deprived, ciliated *CEP78* KO cells display significantly increased centrosomal levels of CEP350
277 (Figure 5A, B) as compared to controls. However, in serum-deprived, non -ciliated cells, the centro-
278 somal levels of CEP350 were not significantly different in *CEP78* KO cells compared to WT con-
279 trols (Figure 5C, D). Similar results were obtained for CEP350 in control and CEP78 deficient pa-
280 tient HSFs (Figure 5E-H). We also analyzed the cellular levels of VPRBP by western blotting and
281 the centrosomal levels of EDD1 by IFM in RPE1 WT and *CEP78* KO cells. Since the VPRBP anti-
282 body cross-reacted with an unknown protein of lower molecular mass in western blot analysis (data
283 not shown) we could not use this antibody to assess centrosomal levels of VPRBP in our cells, but
284 we note that a previous study concluded that CEP78 is not required for VPRBP recruitment to the
285 centrosome [27]. Similarly, we found that VPRBP cellular levels were not significantly increased in
286 serum-fed or serum-deprived *CEP78* KO cells compared to controls (Figure 6A-C). Thus, CEP78
287 seems to be dispensable for recruitment of VPRBP and CEP350 to the centrosome. In contrast, cen-
288 trosomal levels of EDD1 were significantly reduced in RPE1 *CEP78* KO cells compared to WT
289 controls, both in ciliated and non-ciliated cells (Figure 6D-G). Thus, CEP78 is required for efficient
290 recruitment of EDD1 to the centrosome. To corroborate this result, we measured the centrosomal
291 levels of EDD1 in RPE1 *CEP350* KO cells and found that EDD1 levels were also significantly re-
292 duced when compared to the controls (Figure 6-figure supplement 1). Together our data indicate
293 that CEP350, by recruiting CEP78 to the centrosome, also promotes the centrosomal recruitment of
294 EDD1.
295
296 **Increased cellular and centrosomal levels of CP110 in CEP78 deficient cells**
297 Since EDD1 is an E3 ubiquitin-protein ligase that negatively regulates CP110 levels [27], and
298 whose depletion impairs ciliogenesis [39, 40], we asked if the loss of CEP78 would lead to altered
299 levels of CP110 at the centrosome. Indeed, western blot and IFM analysis of RPE1 WT and *CEP78*
300 KO cells revealed that total cellular and centrosomal CP110 levels are significantly increased in

301 *CEP78* KO cells compared to WT controls, both under serum-deprived (Figure 7A-D, F, G) and se-
302 rum-fed conditions (Figure 7-figure supplement 1A-D). We also analyzed CP110 levels specifically
303 at the mother centriole of ciliated RPE1 WT and *CEP78* KO cells and found no significant differ-
304 ences between them (Figure 7E). Similar results were obtained using *CEP78* mutant and control
305 HSF cells (Figure 7G-H). Since a previous study reported that siRNA-mediated depletion of CEP78
306 in RPE1 and HeLa cells reduces the cellular levels of CP110 [27], a result contradicting our own
307 observations (Figure 7; Figure 7-figure supplement 1), we tested if the elevated CP110 levels seen
308 in our *CEP78* mutant cells might be due to compensatory upregulation of CP110 mRNA expres-
309 sion. However, RNA-Seq analysis indicated no significant changes in CP110 mRNA levels in pa-
310 tient-derived, *CEP78* deficient HSF cultures compared to controls; mRNA levels of CEP350,
311 VPRBP and DDB1 in *CEP78* deficient HSF cultures were also similar to those of controls (Figure
312 7-figure supplement 2). We conclude that loss of CEP78 leads to elevated cellular and centrosomal
313 levels of CP110 and that this is not due to upregulation of *CP110* transcription. Furthermore, our
314 results indicate that in ciliated *CEP78* KO cells, the amount of CP110 present specifically at the
315 mother centriole is not significantly higher than in control cells.
316
317 **Partial depletion of CP110 normalizes ciliation frequency of *CEP78* KO cells**
318 CP110 is a key negative regulator of ciliogenesis [5, 41] that was also shown to be required for cili-
319 ogenesis initiation as well as ciliary length control [42, 43]. The above results therefore prompted us
320 to test if the reduced ciliation frequency and/or increased length of remaining cilia observed in
321 *CEP78* deficient cells could result from elevated centrosomal CP110 levels in these cells. Indeed,
322 when we used siRNA to partially deplete CP110 from RPE1 WT and *CEP78* KO cells and sub-
323 jected the cells to serum deprivation, we found that the *CEP78* KO cells restored their ciliation fre-
324 quency to WT level (Figure 8A, B), whereas partial CP110 depletion had little effect on cilia num-
325 bers in WT cells grown under similar conditions (Figure 8C, D). In addition, depletion of CP110
326 from *CEP78* KO cells also seemed to cause a reduction in length of residual cilia, although these
327 cilia were still significantly longer than those of WT controls (Figure 8C, E). Thus, partial depletion
328 of CP110 from *CEP78* KO cells can rescue their reduced ciliation frequency phenotype but likely
329 not the increased length of remaining cilia.
330
331 **Discussion**

332 Several studies have shown that loss-of-function mutations in *CEP78* are causative of ciliopathy
333 characterized by CRDHL [29-32], and that cells lacking CEP78 display reduced ciliation frequency
334 [34] or abnormally long cilia [29, 30]. However, the molecular mechanisms by which CEP78 regu-
335 lates cilium biogenesis and length were so far unclear. In this study, we found that loss of CEP78
336 leads to decreased ciliation frequency as well as increased length of the residual cilia that do form,
337 both in RPE1 cells and patient-derived HSFs. In addition, overexpression of CEP78 in RPE1 cells
338 similarly causes reduced ciliation frequency, as reported previously [27]. The latter observation in-
339 dicates that overexpression of CEP78 has an inhibitory effect on ciliogenesis, possibly by sequester-
340 ing one or more ciliogenic binding partners, e.g. CEP350.
341 Interestingly, our study suggests that both ciliated and non-ciliated CEP78 deficient cells fail
342 to efficiently recruit EDD1 to the centrosome, whereas cellular and centrosomal levels of CP110 are
343 dramatically increased. The increased centrosomal levels of CP110 observed in serum-deprived
344 CEP78 mutant cells likely account, at least in part, for their reduced ciliation frequency, since par-
345 tial depletion of CP110 in these cells could restore ciliation frequency to normal. The removal of
346 CP110 from the distal end of the mother centriole constitutes a key step in the initiation of ciliogen-
347 esis and is regulated by a growing number of proteins that include TTBK2 [19] and components of
348 the UPS system such as Neurl-4 [44] and the cullin-3 (CUL3)–RBX1–KCTD10 complex [45]. The
349 EDD1-DYRK2-DDB1^{VPRBP} complex was similarly shown to mediate degradation of CP110 and to
350 interact with CEP78 [27], but the precise consequences of these activities for ciliogenesis were un-
351 clear. Our work strongly suggests that CEP78 functions together with the EDD1-DYRK2-
352 DDB1^{VPRBP} complex to negatively regulate centrosomal CP110 levels at the onset of ciliogenesis,
353 leading to its removal from the distal end of the mother centriole. This is in contrast to a previously
354 proposed model, which suggested that CEP78 inhibits degradation of CP110 by the EDD1-
355 DYRK2-DDB1^{VPRBP} complex [27]. The reason for this discrepancy is unclear, but may be due to
356 different experimental approaches used in our study and the paper by Hossain et al. [2]. In this latter
357 study, siRNA was used to partially deplete CEP78 from cultured cells, whereas we performed our
358 experiments on cells with endogenous CEP78 mutations. CP110 removal from the distal end of the
359 mother centriole occurs concomitantly with docking of the centriole to vesicles or the plasma mem-
360 brane at the onset of ciliogenesis [12]}. Therefore, a role for CEP78 in removal of CP110 from the
361 centrosome is compatible with ultrastructural analyses in *Planarians*, which indicated that basal
362 bodies fail to dock to the plasma membrane in CEP78 RNAi-depleted animals failure [34]. Alt-
363 hough not addressed in detail in the current study, the elevated centrosomal CP110 levels observed

364 in serum-fed, CEP78 deficient cells are also compatible with previous work implicating CEP78 in
365 regulation of PLK4-mediated centriole duplication [35].
366 We also uncovered a new physical interaction between CEP78 and the N-terminal region of
367 CEP350, and found that CEP350 is important for recruitment of CEP78 to the centrosome as well
368 as for its overall stability. The reduced interaction of the CEP78^{L150S} mutant protein with CEP350
369 might explain its lack of detection by western blot analysis of patient HSFs [30], since reduced in-
370 teraction with CEP350 is likely to decrease the long-term stability of CEP78^{L150S}. Our IP and IFM
371 results furthermore suggests that CEP350 controls CP110 removal from the mother centriole not
372 only via recruitment of TTBK2 [24], but also via CEP78-dependent recruitment of EDD1. Indeed,
373 we observed reduced centrosomal levels of EDD1 in *CEP350* KO cells, consistent with this idea. It
374 remains to be determined whether these two pathways act in sequence or in parallel to control cen-
375 trosomal CP110 levels. Furthermore, as the recruitment of CEP350 to centrioles itself depends on
376 FOP [24, 26, 37] and on the distal centriole protein C2CD3 [14], loss of these proteins may simi-
377 larly affect the centrosomal recruitment of CEP78 and EDD1, and thereby negatively regulate
378 CP110 levels via this pathway. It will be important to investigate these possibilities in future stud-
379 ies.
380 While increased CP110 levels can account for the decreased ciliation frequency observed in
381 serum-deprived CEP78 mutant cells, it remains unclear why some of these cells form abnormally
382 long cilia despite elevated centrosomal and cellular levels of CP110. Our analysis indicated that the
383 ciliated mutant cells are able to locally displace CP110 from the mother centriole, as the amount of
384 CP110 present specifically at the mother centriole/basal body of these cells was the same as for
385 control cells. However, the underlying mechanism remains to be determined. Of note, the *CEP350*
386 KO cells used in our study also appear to be able to overcome increased centrosomal levels CP110
387 during ciliogenesis, since approximately 30% of these cells form cilia despite an inability to recruit
388 TTBK2 and remove CP110 from the mother centriole [24]. It should also be noted that some studies
389 have reported dual roles for CP110 during ciliogenesis, i.e. CP110 may not only function to inhibit
390 ciliogenesis but may also promote ciliary extension in some contexts [42, 43]. Although the mecha-
391 nism responsible for the elongated cilia phenotype seen in some of the CEP78 mutant cells remains
392 unclear, it is interesting that exogenously expressed WT CEP78 as well as CEP78^{L150S} could rescue
393 this phenotype, even though the CEP78^{L150S} mutant protein displayed reduced recruitment to the
394 centrosome. It is likely that in an over-expression context there are sufficient levels of CEP78^{L150S}
395 present at the centrosome to promote ciliary shortening in the mutant cells; alternatively, it might

396 sequester one or more factors in the cytosol needed for ciliary lengthening. One attractive candidate
397 for such a factor is CEP350, which we found to be present at abnormally high levels at the centro-
398 some of ciliated *CEP78* KO cells, specifically.

399 Interestingly, in addition to promoting ubiquitination and degradation of CP110 [27], EDD1
400 was also shown to mediate ubiquitination of CSPP-L in turn promoting its recruitment to centriolar
401 satellites and the centrosome [40]. CSPP-L is a well-known positive regulator of primary cilia for-
402 mation [46] that was recently shown to bind directly to CEP104 to control axoneme extension [47].
403 Furthermore, CEP104 is implicated in ciliogenesis through interaction with the CEP97-CP110 com-
404 plex and modulation of microtubule dynamics at the ciliary tip [47-49]. It will therefore be interest-
405 ing to investigate if and how CSPP-L and CEP104 localization is affected in CEP78 mutant cells.
406 Moreover, as CEP350 additionally binds to CYLD [50], a de-ubiquitinase that controls centriolar
407 satellite homeostasis and ciliogenesis through de-ubiquitination of the E3 ubiquitin ligase MIB1
408 [51, 52], and also regulates axonemal IFT particle injection through FOP-CEP19-RABL2 interac-
409 tions [24-26], it is tempting to speculate that CEP78 might impinge on these processes.
410
411

412 ## Materials and methods

413

414 **Key Resources Table**

Reagent type (species) or resource	Designation	Source or reference	Identifier	Additional information
Cell line (*H. sapiens*)	hTERT-RPE1	ATCC	Cat# CRL-4000	Derived from human retinal pigment epithelium
Cell line (*H. sapiens*)	Puromycin-sensitive hTERT-RPE1	Francesc Garcia-Gonzalo, Autonomous University of Madrid, Madrid, Spain	N/A	
Cell line (*H. sapiens*)	hTERT-RPE1 *CEP78* KO	[30]	N/A	
Cell line (*H. sapiens*)	hTERT-RPE1-BFP-Cas9/pMCB306 (pool)	[24]	N/A	Control cell line for *CEP350* and *FOP* KO lines
Cell line (*H. sapiens*)	hTERT-RPE1-BFP-Cas9/ *CEP350* KO (pool)	[24]	N/A	
Cell line (*H. sapiens*)	hTERT-RPE1-BFP-Cas9/*FOP* KO (pool)	[24]	N/A	
Cell line (*H. sapiens*)	293T	ATCC	Cat# CRL-3216	Derived from human embryonic kidney
Primary cells (*H. sapiens*)	Control skin fibroblasts	[29]	N/A	
Primary cells (*H. sapiens*)	Compound heterozygous skin fibroblasts with two *CEP78* mutations: c.449T>C; p.Leu150Ser and c.1462-1G>T	[30]	F3: II:1	These cells do not express detectable levels of CEP78 [30]

Primary cells (*H. sapiens*)	Compound heterozygous skin fibroblasts with two *CEP78* mutations: c.633delC; p.Trp212Glyfs*18 and c.499+5G>A; IVS + 5G>A	[29]	2702r34, individual II-3	These cells do not express detectable levels of CEP78 [29]
Primary cells (*H. sapiens*)	Homozygous substitution in the first invariant base of intron 3 splice donor site in *CEP78*: c.499+1G>T (IVS3+1G>T)	[29]	KN10, individual II-1	These cells express almost undetectable levels of CEP78 [29]
Bacterial strain (*E. coli*)	DH10B	Lab stock	N/A	
Antibody	Anti-Acetylated-tubulin (mouse monoclonal)	Sigma-Aldrich	Cat# T7451	IFM (1:2000)
Antibody	Anti-α-tubulin (mouse monoclonal)	Sigma-Aldrich	Cat# T5168	WB (1:10000)
Antibody	Anti-ARL13B (rabbit polyclonal)	Proteintech	Cat# 17711-1-AP	IFM (1:500)
Antibody	Anti-CEP78 (rabbit polyclonal)	Bethyl Laboratories	Cat# A301-799A-M	IFM (1:200) WB (1:500)
Antibody	Anti-CEP350 (mouse monoclonal)	Abcam	Cat# Ab219831 (CL3423)	IFM (1:500)
Antibody	Anti-CEP350 (rabbit polyclonal)	Novus Biologicals	Cat# NB100-59811	IFM (1:200)
Antibody	Anti-CP110 (rabbit polyclonal)	Proteintech	Cat# 12780-1-AP	IFM (1:200) WB (1:1500)
Antibody	Anti-DCTN1/P-150 (mouse monoclonal)	BD Biosciences	Cat# 610474	IFM (1:500)
Antibody	Anti-EDD1 (rabbit polyclonal)	Bethyl Laboratories	Cat# A300-573A-M	IFM (1:100)

Antibody	Anti-FLAG (mouse monoclonal)	Sigma-Aldrich	Cat# F1804	IFM (1:500) WB (1:1000)
Antibody	Anti-FLAG (rabbit polyclonal)	Sigma-Aldrich	Cat# F7425	WB (1:1000)
Antibody	Anti-FGFR1OP/FOP (mouse monoclonal)	Novus Biologicals	Cat# H00011116-M01	WB (1:500)
Antibody	Anti-GAPDH (rabbit polyclonal)	Cell Signaling Technology	Cat# 2118	WB (1:1000)
Antibody	Anti-GFP (rabbit polyclonal)	Sigma-Aldrich	Cat# SAB4301138	WB (1:500)
Antibody	Anti-Myc (mouse monoclonal, 9B11)	Cell Signaling Technology	Cat# 2276S	WB (1:1000)
Antibody	Anti-phospho Rb (S807/811) (mouse monoclonal)	Cell Signaling Technology	Cat# 9308	WB (1:500)
Antibody	Anti-VPRBP (rabbit polyclonal)	Bethyl Laboratories	Cat# A301-877A-M	WB (1:200)
Antibody	Polyclonal Goat Anti-Mouse Immunoglobulins /Horseradish Peroxidase conjugated	Dako	Cat# P0447	WB (1:10000)
Antibody	Polyclonal Swine Anti-Rabbit Immunoglobulins /Horseradish Peroxidase conjugated	Dako	Cat# P0399	WB (1:10000)
Antibody	Donkey anti-Mouse IgG (H+L) Highly Cross-Adsorbed Secondary Antibody/Alexa Fluor 488-conjugated	Thermo Fischer Scientific	Cat# A21202	IFM (1:500)

Antibody	Donkey anti-Mouse IgG (H+L) Highly Cross-Adsorbed Secondary Antibody/Alexa Fluor 568-conjugated	Thermo Fischer Scientific	Cat # A10037	IFM (1:500)
Antibody	Donkey anti-Rabbit IgG (H+L) Highly Cross-Adsorbed Secondary Antibody/Alexa Fluor 488-conjugated	Thermo Fischer Scientific	Cat #A21206	IFM (1:500)
Antibody	Donkey anti-Rabbit IgG (H+L) Highly Cross-Adsorbed Secondary Antibody/Alexa Fluor 568-conjugated	Thermo Fischer Scientific	Cat# A10042	IFM (1:500)
Enzyme	USER® Enzyme	New England BioLabs	Cat# M5505L	
Enzyme	Phusion® High-Fidelity DNA polymerase	New England BioLabs	Cat# M0530L	
Recombinant DNA reagent	*H. sapiens* Angiomotin p80 (Ap80)/pCMV-FLAG	[53]	N/A	
Recombinant DNA reagent	*H. sapiens* CEP78 aa 2-217/pEGFP-C1	This study	CEP78 N-terminus (N)	PCR-amplified using primers h.CEP78.4f.kpn1 and hsEGFP-CEP78_Rv (651)
Recombinant DNA reagent	*H. sapiens* CEP78 aa 203-403/pEGFP-C1	This study	CEP78 Middle (M)	PCR-amplified using primers hsEGFP-CEP78_Fwd (607) and hsEGFP-CEP78_Rv (1209)

Recombinant DNA reagent	*H. sapiens* CEP78 aa 2-403/pEGFP-C1	This study	CEP78 N-terminus plus Middle (NM)	PCR-amplified using primers h.CEP78.4f.kpn1 and hsEGFP-CEP78_Rv (1209)
Recombinant DNA reagent	*H. sapiens* CEP78 aa 395-722/pEGFP-C1	This study	CEP78 C-terminus (C)	PCR-amplified using primers hsEGFP-CEP78_Fwd (1186) and hCEP78.rv_stop. bamh1
Recombinant DNA reagent	*H. sapiens* CEP78/pEGFP-C1	This study	N/A	PCR-amplified using primers h.CEP78.4f.kpn1 and hCEP78.rv_stop. bamh1
Recombinant DNA reagent	*H. sapiens* CEP78/pDEST306	This study	p3xFLAG-CEP78	
Recombinant DNA reagent	*H. sapiens* CEP78^{L150S}/pDEST306	This study	p3xFLAG-CEP78^{L150S}	
Recombinant DNA reagent	Plasmid pEGFP-C1 (empty vector)	TaKaRa Bio	Cat# 6084-1	
Recombinant DNA reagent	Gateway® pDONR^{TM}201	Invitrogen/Thermo Fischer Scientific	Cat# 11798-014	
Recombinant DNA reagent	Gateway® pDEST306	Invitrogen/Thermo Fischer Scientific	N/A (lab stock)	Cloning produces in-frame 3xFLAG tag in the N-terminus
Recombinant DNA reagent	*H. sapiens* CEP350 aa 1-983/pCS2^{+} with a 6×myc tag	[50, 54]	CAP N	
Recombinant DNA reagent	*H. sapiens* CEP350 aa 2990-3117/pCS2^{+} with a 6×myc tag	[50, 54]	CAP C	
Recombinant DNA reagent	*H. sapiens* VPRBP/pCMV-Myc	[55]	Myc-VPRBP	Cloned in Sal1 and Not1 sites

Sequence-based reagent	*H. sapiens CEP78* ORF/ GeneCopoiea pShuttle™Gateway® PLUS ORF	GeneCopoiea	NCBI reference Sequence NM_001098802.3	
Sequence-based reagent	*H. sapiens CEP78* PCR primer	Sigma-Aldrich	attB forward	5'-GGGACAAGTTGTACAAAAAACAGGCTTCATCGACTCCGTGAAGCTGC-3'
Sequence-based reagent	*H. sapiens CEP78* PCR primer	Sigma-Aldrich	attB reverse	5-GGGGACCACTTTGTACAAGAAAGCTGGGTTTCAGGAATGCAGGTCCTTTCCAG-3'
Sequence-based reagent	*H. sapiens CEP78* PCR primer	Sigma-Aldrich	CEP78 mut_F	5'-AGAGACAGGTGCACCGAAGAAGCCGATTTATTCAATC-3'
Sequence-based reagent	*H. sapiens CEP78* PCR primer	Sigma-Aldrich	CEP78 mut_R	5'-GATTGAATAAATCGGCTTCTTCGGTGCACCTGTCTCT-3'
Sequence-based reagent	*H. sapiens CEP78* PCR primer	Eurofins Genomics	hCEP78.4f.kpn1	5'-AAGGTACCATCGACTCCGTGAAGCTGCG-3'
Sequence-based reagent	*H. sapiens CEP78* PCR primer	Eurofins Genomics	hsEGFP-CEP78_Rv (651)	5'-AAGGATCCTTAGCGAAGACTCTCAGCCCAG-3'
Sequence-based reagent	*H. sapiens CEP78* PCR primer	Eurofins Genomics	hsEGFP-CEP78_Fwd (607)	5'- GGGGTACCCAGACCATGAGAAGGCATGA -3'

Sequence-based reagent	*H. sapiens CEP78* PCR primer	Eurofins Genomics	hsEGFP-CEP78_Rv (1209)	5'-GGGGATCC TTAACCCCTG TGTCTTTTTGC AC-3'
Sequence-based reagent	*H. sapiens CEP78* PCR primer	Eurofins Genomics	hsEGFP-CEP78_Fwd (1186)	5'-GGGGTACC GCAGAACGTG CAAAAAGACA -3'
Sequence-based reagent	*H. sapiens CEP78* PCR primer	Eurofins Genomics	hCEP78.rv_stop. bamh1	5'-GAGGATCC ACAGGAATGC AGGTCCTTTC-3'
Sequence-based reagent	Control siRNA	Eurofins Genomics	N/A	5'-UAAUGUAUU GGAAGGCA-3'
Sequence-based reagent	*H. sapiens CP110* siRNA	Eurofins Genomics /[5]	N/A	5'-GCAAAACCAG AAUACGAGAT T-3'
Chemical compound	DAPI (4′, 6-diamidino-2-phenylindole)	Thermo Fischer Scientific	Cat# D1306	Stored at -20ºC as stock solution of 20 µg/ml in H_2O
Chemical compound	FuGENE®6	Promega	Cat# E2692	
Chemical compound	DharmaFECT™ Duo Transfection reagent	Dharmacon™	Cat# T-2010-03	
Software/ algorithm	cellSens Dimension	Olympus	Version 1.18	
Software/ algorithm	Zen Black 2012	Zeiss	Version 2012	
Software/ algorithm	Adobe Photoshop®	Adobe	Version 21.0.1	
Software/ algorithm	Adobe Illustrator®	Adobe	Version 24.2.1	
Software/ algorithm	ImageJ	NIH	Mac OS X or Windows	
Software/ algorithm	GraphPad Prism 6.0	GraphPad Software Inc.	Mac OS X or Windows	
Software/ algorithm	MaxQuant	[56]	Version 1.6.1.0	

Other	Anti-FLAG® M2 Affinity Gel	Sigma-Aldrich	Cat# A2220	
Other	Anti-c-Myc Agarose Affinity Gel antibody produced in rabbit	Sigma-Aldrich	Cat# A7470-1 ml	
Other	GFP-Trap® Agarose	ChromoTek GmbH	Cat# gta-20	
Other	QuickChange Lightning Site-Directed Mutagenesis Kit	Agilent	Cat# 210518	
Other	Direct-zol RNA Miniprep Kit	Zymo Research	Cat# R2051	
Other	Agilent RNA Nano 6000 Assay Kit	Agilent	Cat# 5067-1511	
Other	NEBNext® Ultra™ RNA Library Prep Kit for Illumina®	New England BioLabs	Cat# E7530L	
Other	Invitrogen™ Qubit® RNA Assay Kit	Thermo Fischer Scientific	Cat# 32852	
Other	AMPure XP system	Beckman Coulter Life Sciences	Cat# A63881	

415

416 **PCR and cloning**

417 For the establishment of the N-terminal FLAG-tagged CEP78 construct a cDNA clone coding for
418 human full-length CEP78 cDNA (GeneCopoiea pShuttle™Gateway® PLUS ORF, NCBI accession
419 number NM_001098802) was used as template for amplification with the Phusion High-Fidelity
420 DNA polymerase (New England BioLabs) under standard PCR conditions and attB forward and re-
421 verse primers (see Key Resources Table) compatible with the Gateway cloning technology (Invitro-
422 gen/Thermo Fisher Scientific) for inclusion of the insert into the pDonor201 Gateway vector (Invi-
423 trogen/Thermo Fischer Scientific). To produce human FLAG-CEP78^{L150S}, site directed mutagenesis
424 was performed with QuickChange Lightning Site-Directed Mutagenesis Kit (Agilent) and primers
425 CEP78 mut_F and CEP78 mut_R (see Key Resources Table). Accuracy of the *CEP78* ORF was
426 assessed by Sanger sequencing. Subsequently, the desired fragment was cloned into the pDEST306
427 vector (Invitrogen/Thermo Fisher Scientific.

428 Plasmids encoding full-length and truncated versions (N-terminus, middle, N-terminus plus
429 middle, C-terminus) of CEP78 tagged with GFP in the N-terminus were generated by PCR using
430 relevant primers (see Key Resources Table) and pFLAG-CEP78 as template; PCR products were
431 cloned into pEGFP-C1 by standard approaches, following digestion with BamHI (Roche, cat#
432 1056704001) and KpnI (Roche, cat#10899186001) and ligation with T4 DNA ligase (Applichem,
433 cat# A5188). Ligated plasmids were transformed into competent *E. coli* DH10B cells and cells har-
434 boring recombinant plasmids selected on Luria Bertani (LB; Sigma-Aldrich) agar plates with 50
435 µg/ml kanamycin. Plasmids were purified using Plasmid DNA Mini Kit I (Omega Biotech, cat#
436 D6943-02) or Nucleobond Xtra Mid kit (Macherey-Nagel, cat# 740410.50), according to protocols
437 supplied by the manufacturers. Sequences of plasmid inserts were verified by Eurofins Genomics.
438
439 **Mammalian cell culture and transfection**
440 Human skin fibroblasts were cultured as described previously [29, 30]. Human embryonic kidney-
441 derived 293T cells were cultured and transfected with plasmids as described previously [57]. RPE1
442 cells were grown in T-75 flasks in a 95% humidified incubator at 37 ºC with 5% CO2. Cells were
443 cultured in Dulbecco's Modified Eagle Medium (DMEM) (GIBCO®, cat# 41966-029) supple-
444 mented with 10% fetal bovine serum (FBS) and 1% penicillin/streptomycin (P/S). When cells were
445 about 80-90% confluent, they were passaged and set up for new experiments. Upon seeding, RPE1
446 cells were washed once with preheated 1 x phosphate buffered saline (PBS) and then incubated with
447 1% Trypsin-EDTA (ethylenediaminetetraacetic acid) (Sigma-Aldrich, cat# T4174) solution for 5
448 min at 37 ºC. The detached cells were aspired in an appropriate volume of new preheated DMEM
449 and seeded into petri dishes with or without sterile glass coverslips [58]. When the cells had reached
450 80-90% confluency they were serum starved for 24 hours to induce formation of primary cilia. A
451 small amount of cell solution was passaged on in a new T-75 flask containing new preheated
452 DMEM.
453 For transfection with plasmids, RPE1 cells were seeded in 60 mm petri dishes as described
454 above to about 50-70% confluency at the time of transfection. For rescue experiments, 2 µg
455 pFLAG-CEP78 or pFLAG-CEP78^{L150S} and 6 µl FuGENE®6 were mixed in 100 µl serum- and anti-
456 biotic free DMEM and incubated for 20 minutes at room temperature. New DMEM was added to
457 the cells prior to transfer of the transfection reagent, which was gently dripped onto the cells and
458 swirled to make sure it was dispersed well. After cells were incubated with transfection medium
459 for 4 hours, the medium was replaced with serum free DMEM for 24 hours to induce growth arrest.

460 Gene silencing in RPE1 cells by siRNA was performed using DharmaFect (see Key Resources Ta-
461 ble). Briefly, RPE1 cells were seeded in DMEM medium with serum and antibiotics in 30 mm petri
462 dishes at 20-25% confluency. Transfection was performed by combining 50 nM siRNA with 5 µl of
463 DharmaFect in 200 µl of serum and antibiotic-free DMEM medium for 15 min at room tempera-
464 ture. After incubation, the complexes were added dropwise onto the cells and the media was swirled
465 gently to ensure good dispersion prior to incubation at 37 °C. Cells were kept under these condi-
466 tions for 48 hours and then serum starved for 24 hours before being processed for further experi-
467 ments.
468
469 **Immunofluorescence microscopy and image analysis**
470 Standard epifluorescence IFM analysis was performed as described previously [58]. Briefly, glass
471 coverslips containing cells of interest were washed in PBS and fixed with either 4% paraformalde-
472 hyde (PFA) solution for 15 min at room temperature or on ice, or with ice-cold methanol for 12-15
473 min at -20 ºC. After three washes in PBS the PFA-fixed cells were permeabilized 10 min in 0.2%
474 Triton X-100 and 1% Bovine Serum Albumin (BSA) in PBS and blocked in 2% BSA in PBS for 1
475 hour at room temperature. Coverslips were incubated over night at 4 ºC in primary antibodies (see
476 Key Resources Table) diluted in 2% BSA in PBS. The next day, coverslips were washed three
477 times with PBS for 5 min and incubated for 1 hour at room temperature in secondary antibodies
478 (see Key Resources Table) diluted in 2% BSA in PBS. Coverslips were washed three times in PBS
479 for 5 min before staining with 2 µg/ml DAPI solution PBS for 30 sec. Finally, coverslips were
480 washed once with PBS and before mounting on objective glass with 6% n-propyl gallate diluted in
481 glycerol and 10x PBS and combined with Shandon™ Immuno-Mount™ (Thermo Scientific, cat#
482 9990402) in a 1:12 ratio. Cells were imaged on a motorized Olympus BX63 upright microscope
483 equipped with a DP72 color, 12.8 megapixel, 4140 x 3096 resolution camera. cellSense Dimension
484 software 1.18 from Olympus was used to measure cilia length; ImageJ version 2.0.0-rc-69/1.52i
485 was used to measure the relative mean fluorescence intensity (MFI) of relevant antibody-labeled
486 antigens at the centrosome/basal body. Images were first converted to 8 bit (grayscale) so that the
487 intensity of the histogram always was constant between 0-255. A fixed circle was drawn around a
488 centrosome in a cell. This same region of interest (ROI) was used to measure the MFI of a specific
489 protein at the centrosome. A constant ROI was also drawn to measure the cell background signal
490 which was subtracted from the MFI measured at the centrosome/basal body. Images were prepared
491 for publication using Adobe Photoshop® and Adobe Illustrator®.

492 For super resolution imaging, RPE1 cells were photographed on a 3D-SIM Zeiss Elyra PS.1
493 microscope equipped with 488 and 561 nm diode lasers, two high-speed sCMOS pco-edge cameras
494 (scientific sCMOS 16-bit depth; 1280 x1280 pixel resolution; 0.04 µm pixel size, manufactured by
495 PCO), and a x100/ 1.46 NA alpha Plan-Apochromat oil immersion DIC M27 objective (Zeiss).
496 Multi-channel 3D-SIM image Z-stacks were acquired with three rotations of the grid and with 0.116
497 µm interval between each section. SIM images were reconstructed using Zeiss Zen Black 2012 soft-
498 ware. After acquisition, channel alignment was performed using calibrations based on GE reference
499 slide containing 100 nm diameter TetraSpeck Microspheres and the Z-stacks were three-dimension-
500 ally reconstructed using ImageJ (v 1.53c).
501
502 **Statistical analysis**
503 Statistical analyses were performed using GraphPad Prism 6.0. The background-corrected MFI
504 measured at the centrosome was normalized to relevant control cells. Mean and standard deviation
505 (SD) was calculated for all groups, and outliers were identified and removed by the ROUT method
506 before the statistical tests were conducted. The data was tested for normality using either D'Ago-
507 stino's K-squared test or Shapiro-Wilk test. Depending on the distribution of the data, two-tailed
508 and unpaired Student's t-test or Mann Whitney test were used when comparing two groups. One-
509 way ANOVA followed by Tukey's or Dunn's multiple comparison was used when comparing more
510 than two groups. Unless otherwise stated, the statistical analyses were performed on at least three
511 independent biological replicates (n=3). A p-value under 0.05 was considered statistically signifi-
512 cant and p-values are indicated in the figures with asterisks as follows; * $p<0.05$, ** <p0.01,
513 ***<0.001, and **** $p<0.0001$.
514
515 **Immunoprecipitation (IP), protein quantification, SDS-PAGE and western blot analysis**
516 Immunoprecipitation of transfected 293T cell lysates was performed as described previously [57]
517 using relevant antibody-conjugated beads (see Key Resources Table). Protein concentrations were
518 measured using the *DC*™ Protein Assay Kit I from Bio-Rad (cat # 5000111) by following the man-
519 ufacturer's protocol. For SDS-PAGE analysis of RPE1 and HSF cells, protein samples were pre-
520 pared by lysis of cells with 95 ºC SDS-lysis buffer (1% SDS, 10 mM Tris-HCl, pH 7.4) and cell ly-
521 sates transferred to Eppendorf tubes and heated shortly at 95 ºC. The samples were then sonicated
522 two times for 30 seconds to shear DNA followed by centrifugation at 20,000 x *g* for 15 min at room

523 temperature to pellet cell debris. Supernatants were transferred to new Eppendorf tubes and an ali-
524 quot of each sample used for determination of protein concentration. Samples with equal concentra-
525 tions of protein were prepared for SDS-PAGE analysis by addition of NuPAGE™ LDS Sample
526 Buffer (4X) from Thermo Fischer Scientific (cat# NP0007) and 50 mM DTT. Samples from IP
527 analysis in 293T cells, performed using modified EBC buffer [57], were prepared for SDS-PAGE in
528 a similar fashion. Protein samples were heated at 95 ºC for 5 minutes before loading them on a
529 Mini-PROTEAN® TGX™ Precast Gel 4-15% from Bio-Rab Laboratories, Inc. (cat# 456-1083 or
530 cat #456-1086). PageRuler™ Plus Prestained Protein Ladder (Thermo Fischer Scientific, cat#
531 26619) was used as molecular mass marker. SDS-PAGE was performed using the Mini-PRO-
532 TEAN® Tetra System from Bio-Rad. Gels were run at 100 V for 15 minutes and 200 V for 45
533 minutes. Using the Trans-BLOT® Turbo Transfer System from Bio-Rad Laboratories, Inc. the pro-
534 teins were transferred at 1.3 A, 25 V for 10 min from the gel to a Trans-Blot® Turbo™ Transfer
535 Pack, Mini format 0.2 µm Nitrocellulose membrane (cat# 1704158). Ponceau-S solution was added
536 to the membrane to visualize the proteins before blocking in 5% milk in Tris-buffered saline with
537 Tween-20 (TBS-T; 10 mM Tris-HCl, pH 7.5, 150 mM NaCl, 0.1% Tween-20) for 2 hours at room
538 temperature. Primary antibodies (see Key Resources Table) were diluted in 5% milk in TBS-T and
539 incubated with the membrane overnight at 4ºC. The membrane was washed three times 10 min at
540 room temperature in TBS-T on a shaker before incubation with secondary antibody (see Key Re-
541 sources Table), diluted in 5% milk in TBS-T, for 1 hour at room temperature. The membrane was
542 washed three times 10 min at room temperature in TBS-T on a shaker. Finally, SuperSignal™ west
543 Pico PLUS chemiluminescent Substrate (Thermo Scientific, cat # 34580) was mixed in a 1:1 ratio
544 and added to the membrane for 5 min before development on a FUSION FX SPECTRA machine
545 from Vilber.
546
547 **Quantitative mass spectrometry (MS) and peptide identification**
548 For SILAC-based mass spectrometry, three distinct SILAC culture media were used: light-light-
549 (Lys0 and Arg0); medium- (Lys4 and Arg6) and high-labeled media (Lys8 and Arg10). 293T cells
550 were seeded in 100 mm petri dishes and SILAC labeled for 1 week to ensure proper amino acid in-
551 corporation. After the incorporation phase, the cells were transfected with 2 µg of plasmid encoding
552 FLAG-Ap80 (control), FLAG-CEP78 or FLAG-CEP78^{L150S} using 6 µl FuGENE®6, as described
553 above, and then subjected to lysis using modified EBC buffer [56] and FLAG IP as described
554 above. Affinity enriched proteins were digested with trypsin and the resulting peptides desalted

555 prior to LCMS analysis using an Easy-nLC 1000 system (Thermo Scientific) connected to a Q Ex-
556 active HF-X mass spectrometer (Thermo Scientific). Peptides were separated by a 70 minutes gra-
557 dient using increased buffer B (95% ACN, 0.5% acetic acid). The instrument was running in posi-
558 tive ion mode with MS resolution set at 60,000 for a scan range of 300 to 1700 m/z. Precursors
559 were fragmented by higher-energy collisional dissociation (HCD) with normalized collisional en-
560 ergy of 28 eV. For protein identification and quantitation, the obtained MS raw files were processed
561 by MaxQuant software version 1.6.1.0 [56] and searched against a FASTA file from UniProt.
562
563 **RNAseq analysis**
564 RNA was extracted using the Direct-zol RNA Miniprep Kit (Zymo Research) following the manu-
565 facturer's instructions. RNA degradation and contamination were monitored on 1% agarose gels.
566 RNA purity was checked using the NanoPhotometer® spectrophotometer (IMPLEN, CA, USA).
567 RNA concentration was measured using Invitrogen™ Qubit® RNA Assay Kit in Qubit® 2.0 Fluo-
568 rometer (Thermo Fischer Scientific). RNA integrity was assessed using the Agilent RNA Nano
569 6000 Assay Kit of the Bioanalyzer 2100 system (Agilent, CA, USA). A total amount of 3 μg RNA
570 per sample was used as input material for the RNA sample preparations. Sequencing libraries were
571 generated using NEBNext® Ultra™ RNA Library Prep Kit for Illumina® (New England BioLabs,
572 USA) following manufacturer's recommendations and index codes were added to attribute se-
573 quences to each sample. Briefly, mRNA was purified from total RNA using poly-T oligo-attached
574 magnetic beads. Fragmentation was carried out using divalent cations under elevated temperature in
575 NEBNext First Strand Synthesis Reaction Buffer（5X). First strand cDNA was synthesized using
576 random hexamer primer and M-MuLV Reverse Transcriptase（RNase H -）. Second strand cDNA
577 synthesis was subsequently performed using DNA Polymerase I and RNase H. Remaining over-
578 hangs were converted into blunt ends via exonuclease/polymerase activities. After adenylation of 3'
579 ends of DNA fragments, NEBNext Adaptor with hairpin loop structure were ligated to prepare for
580 hybridization. In order to select cDNA fragments of preferentially 150~200 bp in length, the library
581 fragments were purified with AMPure XP system (Beckman Coulter Life Sciences). Then 3 μl
582 USER® Enzyme (New England BioLabs) was used with size-selected, adaptor-ligated cDNA at
583 37°C for 15 min followed by 5 min at 95 °C before PCR. Then PCR was performed with Phusion®
584 High-Fidelity DNA polymerase, Universal PCR primers and Index (X) Primer (New England Bi-
585 oLabs). At last, PCR products were purified (AMPure XP system) and library quality was assessed
586 on the Agilent Bioanalyzer 2100 system. The clustering of the index-coded samples was performed

587 on a cBot Cluster Generation System using HiSeq PE Cluster Kit cBot-HS (Illumina) according to
588 the manufacturer's instructions. After cluster generation, the library preparations were sequenced on
589 an Illumina Hiseq platform and 125 bp/150 bp paired-end reads were generated. Raw data (raw
590 reads) of fastq format were firstly processed through in-house perl scripts. In this step, clean data
591 (clean reads) were obtained by removing reads containing adapter, reads containing ploy-N and
592 lowquality reads from raw data. At the same time, Q20, Q30 and GC content the clean data were
593 calculated. All the downstream analyses were based on the clean data with high quality. Reference
594 genome and gene model annotation files were downloaded from genome website directly. Index of
595 the reference genome was built using Bowtie v2.2.3 [59] and paired-end clean reads were aligned to
596 the reference genome using TopHat v2.0.12 [60]. We selected TopHat as the mapping tool for that
597 TopHat can generate a database of splice junctions based on the gene model annotation file and thus
598 a better mapping result than other non-splice mapping tools. HTSeq v0.6.1 [61] was used to count
599 the reads numbers mapped to each gene and then Fragments Per Kilobase of transcript sequence per
600 Millions base pairs sequenced (FPKM) of each gene was calculated based on the length of the gene
601 and reads count mapped to this gene. FPKM considers the effect of sequencing depth and gene
602 length for the reads count at the same time, and is currently the most commonly used method for
603 estimating gene expression levels [62]. Prior to differential gene expression analysis, for each se-
604 quenced library, the read counts were adjusted by edgeR program package through one scaling nor-
605 malized factor [63]. Differential expression analysis of two conditions was performed using the
606 DEGSeq R package (1.20.0) [64].
607
608 **Acknowledgements**
609 We thank Søren Lek Johansen and Maria Schrøder Holm for expert technical assistance, Benedicte
610 Schultz Kappel and Frida Roikjer Rasmussen for help with plasmid generation, and Nynne Chris-
611 tensen, Center for Advanced Bioimaging (CAB) Denmark, for help with 3D-SIM. We are grateful
612 to Drs. Peter K. Jackson, Tomoharu Kanie, Francesc Garcia-Gonzalo, Laurence Pelletier, Brian Da-
613 vid Dynlacht, Anne-Marie Tassin, Maria Gavilan, Rosa M. Rios, Éric A. Cohen and Peter ten Dijke
614 for reagents. This study was supported grants from Independent Research Fund Denmark (#8020-
615 00162B to PF and LBP, and #8021-00425A to JSA), from the Carlsberg Foundation (#CF18-0294
616 to LBP) and from the Swiss National Science Foundation (#176097 to CR).
617
618 **Author contributions**

619 ABG, Performed experiments, Analyzed the data, Prepared the figures; BBJ, Performed experi-
620 ments, Analyzed the data, Contributed to manuscript preparation; SKH, PM, SKO, MQ, KN,
621 MPDJ, CW, Performed experiments, Analyzed the data; STC, Contributed to manuscript prepara-
622 tion; SP, Analyzed data, Contributed to figure preparation; CR, JSA, Contributed to manuscript
623 preparation, Obtained funding; PF, Conception and design, Performed experiments, Contributed to
624 manuscript preparation, Obtained funding; LBP, Conception and design, Prepared the figures,
625 Wrote the manuscript, Obtained funding.
626
627 **Additional files**
628 Source data for Figure 3A
629 Source data for Figure 7-figure supplement 2
630
631 **Figure 1.** CEP78 mutant cells display fewer, but longer primary cilia. (**A**) Representative IFM im-
632 ages of serum-deprived RPE1 WT and *CEP78* KO cells stained with the indicated antibodies; DAPI
633 marks the nucleus. Scale bar, 5μm. (**B**, **C**) Quantification of the percentage of ciliated cells (**B)** and
634 the length of residual cilia (**C)** in WT and *CEP78* KO cells, based on images as shown in (A). Data
635 were normalized in relation to WT values. Student's t-test (two-tailed, unpaired) was used for the
636 statistical analysis. Graphs in (B) represent accumulated data from three individual experiments
637 (n=384 for WT and n=322 for *CEP78* KO cells). Graphs in (C) show data from three individual ex-
638 periments (n=338 for WT and n=198 for *CEP78* KO cells). (**D**) Representative IFM images of se-
639 rum-deprived control and *CEP78* mutant (Patient) HSFs stained with the indicated antibodies;
640 DAPI marks the nucleus. Scale bar, 5 μm. (**E**, **F**) Quantification of the percentage of ciliated cells
641 (**E**) and the length of residual cilia (**F**) in control and *CEP78* patient HSFs (data from HSFs derived
642 from patient 2702r34, individual II-3 [29]), based on images as shown in (D). Graphs in (E) repre-
643 sent accumulated data from seven individual experiments (n= 678 for control HSFs; n= 707 for pa-
644 tient-derived HSFs). Graphs in (F) show data from seven individual experiments (n= 237 for con-
645 trol HSFs; n= 216 for patient-derived HSFs). Data were normalized in relation to control values. A
646 Student's t-test (unpaired, two-tailed) was performed to address differences in the ciliary frequency
647 and length between control and patient HSFs. (**G**) Western blot analysis of Rb phosphorylated on
648 S807/811 (P-Rb) in RPE1 WT and *CEP78* KO cells grown with or without serum. (**H**, **I**) Quantifi-
649 cation of data shown in (G) from three independent experiments analyzed in duplicates. (**J**) P-Rb
650 blots from HSFs derived from control and patient HSFs grown with or without serum (data from

651 HSFs derived from patient F3: II:1; [30]). GAPDH was used as a loading control. (**K, L**) Quantifi-
652 cation of data shown in (J) from three independent experiments analyzed in duplicates. Student's t-
653 test (two-tailed, unpaired) was used for the statistical analysis in (H, I) and (K, L). Error bars of
654 graphs represent SD and data are shown as mean ± SD. a.u., arbitrary units; (*) $p<0.05$; (****)
655 $p<0.0001$; n.s., not statistically significant.
656
657 **Figure 2.** Analysis of RPE1 WT and *CEP78* KO cells expressing FLAG-CEP78 and FLAG-
658 CEP78^{L150S}. (**A**) Representative IFM images of serum-starved WT and *CEP78* KO cells transiently
659 expressing FLAG-CEP78 and FLAG-CEP78^{L150S} labeled with antibodies against FLAG (green) and
660 ARL13B (magenta). Insets show enlarged views of the cilia-centrosome region. Scale bars: 5 μm in
661 original images and 1 μm in magnified images. (**B**) Quantification of the relative MFI of FLAG-
662 CEP78 and FLAG-CEP78^{L150S} at the centrosome in serum-starved WT cells. Accumulated data from
663 three individual experiments (n=145 and n=151 for cells transfected with FLAG-CEP78 and FLAG-
664 CEP78^{L150S}, respectively). Student's t-test (two-tailed, unpaired) was used for the statistical analysis.
665 Data is shown as mean ±SD. (**C**) Quantification of the percentage of ciliated cells in serum-deprived
666 WT and *CEP78* KO cells expressing the indicated FLAG fusions shown in (A). (**D**) Quantification
667 of the ciliary length in the same group of cells grown in the same conditions mentioned above. Anal-
668 ysis on cilia numbers and size was performed through accumulated data from three independent ex-
669 periments (n=338 for untransfected WT; n=69 for WT+FLAG-CEP78; n=66 for WT+FLAG-
670 CEP78^{L150S}; n=198 for untransfected *CEP78* KO; n=35 for *CEP78* KO + FLAG-CEP78; n=16 for
671 *CEP78* KO + FLAG-CEP78^{L150S}). Ordinary one-way ANOVA with Dunnett's multiple comparison
672 test was used for the statistical analysis of the ciliary frequency and length amongst all groups, in
673 relation to untransfected WT cells mean (control group). Error bars in (C) indicate SD and data in
674 (D) is presented as mean ± SD. Differences in cilia numbers and size between transfected and un-
675 transfected *CEP78* KO cells were assessed by Ordinary one-way ANOVA with Dunnett's multiple
676 comparison test in which the untransfected *CEP78* KO cells were selected as the control group. a.u.,
677 arbitrary units; (*) $p<0.05$; (**) $p<0.01$; (***) $p<0.001$; (****) $p<0.0001$; n.s., not statistically sig-
678 nificant.
679
680 **Figure 3.** CEP78 interacts with the EDD-DYRK2-DDB1^{VPRBP} complex and CEP350. (**A**) Overview
681 of results from CEP78 interactome analysis in 293T cells grown in SILAC medium. Cells expressing
682 FLAG-CEP78 WT, FLAG-CEP78^{L150S} or FLAG-Ap80 (negative control) were subjected to FLAG

683 IP and pellets analyzed by mass spectrometry. The upper panel displays affinity enrichment of Cep78
684 and interaction partners in FLAG-CEP78 WT cells relative to control cells. The lower panel shows
685 how the CEP78^{L150S} mutation weakens these interactions relative to CEP78 WT using ratios normal-
686 ized for equal affinity enrichment of FLAG-tagged CEP78. (**B-D**) 293T cells expressing the indicated
687 Myc-, FLAG-, or GFP-fusions were subjected to IP with anti-FLAG (**B**) or -GFP (**C**, **D**) beads and
688 input and pellet fractions analyzed by SDS-PAGE and western blotting with Myc, FLAG or GFP
689 antibodies as indicated. FLAG-Ap80-NB used in (B) is a negative control. Molecular mass markers
690 are indicated in kDa to the left of the blots. (**E**) Schematic of the CEP350 and CEP78 fusions used in
691 IP analysis. LRR, leucine-rich repeat; CC, coiled coil. The CEP350 constructs were described in [50,
692 54]; the CEP78 constructs were generated in this study based on published sequence information [27,
693 30, 35]. N, N-terminal region; M, middle region; NM, N-terminal plus middle region; C, C-terminal
694 region; FL, full length.
695
696 **Figure 4.** CEP350 regulates stability and centrosomal recruitment of CEP78. (**A**) 3D-SIM analysis
697 of CEP78 localization in serum-deprived WT RPE1 cells. Cells were fixed with PFA and stained
698 with the indicated antibodies. (**B**) Western blot analysis of CEP78 and α-tubulin (loading control)
699 in serum-deprived hTERT-RPE1-BFP-Cas9 control (pMCB306), *CEP350* KO or *FOP* KO cells
700 [24]. (**C**) Quantification of data in (B), based on three independent experiments analyzed in dupli-
701 cates. Error bars indicate SD. Statistical analysis was done using Student's t-test (unpaired, two-
702 tailed). (**D, F**) IFM analysis of serum-deprived control and *CEP350* KO ciliated (D) and non-cili-
703 ated cells (F) using antibodies as indicated. Dashed boxes indicate cropped images to highlight the
704 centrosomal/ciliary area. Scale bars: 5 µm in representative images and 1 µm in insets. (**E, G**)
705 Quantification of the relative MFI of CEP78 at the centrosome in serum-starved, ciliated (E) and
706 non-ciliated (G) control and *CEP350* KO cells, based on images as shown in (D) and (G), respec-
707 tively. Statistical analysis was done using a two-tailed and unpaired Mann-Whitney test for ciliated
708 cells and two-tailed and unpaired Student's t-test. Accumulated data from three individual experi-
709 ments (n=128 and 132 for control and *CEP350* KO ciliated cells, respectively; n= 101 and 107 for
710 control and *CEP350* KO non-ciliated cells, respectively). a.u., arbitrary units; (*) $p<0.05$; (**)
711 $p<0.01$; (****) $p<0.0001$.
712
713 **Figure 5.** Altered centrosomal levels of CEP350 in *CEP78* mutant cells. (**A, C, E, G**) Representa-
714 tive IFM images of ciliated (**A**) and non-ciliated (**C**) serum-deprived RPE1 WT and *CEP78* KO

715 cells, and ciliated (**E**) and non-ciliated (**G**) serum-deprived control and CEP78 deficient (Patient)
716 HSFs (combined data from HSFs from patient F3: II:1 [30] and patient 2702r34, individual II-3
717 [29]) labeled with antibodies indicated in the figure. Insets show closeups of the centrosomal/ciliary
718 area (dashed boxes). Scale bars: 5 µm in representative images and 1 µm in closeups. (**B, D**). Quan-
719 tification of CEP350 relative MFI at the centrosome based on images as shown in (A, C). Data is
720 shown as mean ± SD. A Student's t-test was used as statistical analysis between the two groups
721 based on three individual experiments (n=157 or 158 for ciliated cells; n=144-152 for non-ciliated
722 cells). (**F, H)** Quantification of CEP350 relative MFI at the centrosome in HSFs based on images
723 as shown in (E, G). Data is shown as mean ± SD. Student's t-test was used as statistical analysis be-
724 tween the two cell groups based on seven individual experiments with a total of 154-156 analyzed
725 ciliated cells (**F**), and three individual experiments with a total of 122-126 analyzed non-ciliated
726 cells (**H**). a. u., arbitrary units; n.s, not statistically significant; (****) $p<0.0001$.
727
728 **Figure 6.** Analysis of EDD-DYRK2-DDB1^{VPRBP} complex components in CEP78 deficient cells.
729 (**A**) Western blot analysis of VPRBP in lysates from serum-fed and serum-deprived RPE1 WT and
730 *CEP78* KO cells. α-tubulin was used as a loading control (**B, C**) Quantification of the VPRBP rela-
731 tive levels in the different conditions depicted in (A). Statistical analysis was performed using a
732 Student's t-test (unpaired, two-tailed) from five independent experiments analyzed in duplicates.
733 Error bars indicate SD. (**D, F)** Representative IFM images of ciliated (**D**) and non-ciliated (**F**) se-
734 rum-deprived RPE1 WT and *CEP78* KO cells labeled with antibodies against EDD1 (green) and
735 DCTN1 plus acetylated tubulin (magenta). DAPI was used to mark the nucleus (blue). Insets show
736 enlarged views of the cilium-centrosome region. Scale bars: 5 µm in original images and 1 µm in
737 closeups. (**E, G)** Quantification of the EDD1 MFI at the centrosome based on images as shown in
738 (D) and (F) using a two-tailed and unpaired Student's t-test. Data is shown as mean ± SD. Student's
739 t-test was used from three independent experiments (n=194 and n=201 for ciliated WT and *CEP78*
740 KO cells, respectively; n=194 and n=217 for non-ciliated WT and *CEP78* KO cells, respectively).
741 a.u., arbitrary units; n.s., not statistically significant; (****) $p<0.0001$.
742
743 **Figure 7.** CEP78 deficient cells display elevated cellular and centrosomal levels of CP110. (**A**)
744 Western blot analysis of lysates from serum-deprived RPE1 WT and *CEP78* KO cells using indi-
745 cated antibodies. GAPDH was used as a loading control. (**B**) Quantification of the data shown in

746 (A), based on four independent experiments analyzed in duplicates. Error bars indicate SD. Statisti-
747 cal analysis was done using Student's t-test (unpaired, two-tailed). (**C, F**) Representative IFM im-
748 ages of serum-starved ciliated (**C**) and non-ciliated (**F**) RPE1 WT and *CEP78* KO cells labeled with
749 antibodies against CP110 (green), combined DCTN1 and acetylated tubulin (Ac-tub; magenta) and
750 DAPI to mark the nucleus (blue). Insets show enlarged views of the cilium-centrosome area. Scale
751 bars: 5 µm in original images and 1 µm in closeups. (**D, G**) Quantification of the relative MFI of
752 CP110 at the centrosome based on images as shown in (C) and (F), respectively. Student's t-test
753 (unpaired, two-tailed) from three independent biological experiments (n= 90 and n=75 for ciliated
754 RPE1 WT and *CEP78* KO cells, respectively; n=75 and n=82 for non-ciliated RPE1 WT and
755 CEP78 KO cells, respectively) was used for statistical analysis. Data is presented as mean ± SD. (**E**)
756 Quantification of the relative MFI of CP110 at the mother centriole based on images shown in (C)
757 Mann Whitney test (two-tailed and unpaired) was used as statistical analysis based on two inde-
758 pendent experiments (n=61 and n=62 for RPE1 WT and CEP78 KO cells, respectively). Data is
759 presented as mean ± SD. (**H**) Representative IFM images of serum-deprived healthy and CEP78 de-
760 ficient (Patient) HSFs (data from patient 2702r34, individual II-3 described in [29]) labeled with the
761 indicated antibodies. DAPI was used as counterstaining to mark the nucleus. Dashed lines show
762 closeup images of the centrosome region. Scale bars: 5 µm in original images and 1 µm in closeups.
763 (**I**) Quantification based on observations of 151 and 155 cells of CEP78 control and patient cells,
764 respectively, from three individual experiments. Student's t-test (unpaired and two-tailed) was used
765 to assess differences between the two groups. a.u., arbitrary units; n.s., not statistically significant;
766 (**) $p<0.01$; (***) $p<0.001$; (****) $p<0.0001$.
767
768 **Figure 8.** Depletion of CP110 from *CEP78* KO cells rescues their ciliation frequency phenotype.
769 (**A**) Representative western blots of RPE1 WT or *CEP78* KO cells treated with control (siMock) or
770 CP110-specific siRNA (siCP110). Cells were deprived of serum and blots were probed with anti-
771 body against CP110 or α-tubulin (loading control). (**B**) Quantification of relative cellular CP110
772 levels under different conditions based on blots as shown in (A) (n=3 for WT and n=4 for *CEP78*
773 KO cells; each sample was analyzed in duplicates). Data is represented as mean ±SD. A Student's t-
774 test was used to infer CP110 knock down efficiency between WT cells treated with siMock and
775 siCP110. The same statistical method was applied to the *CEP78* KO cells treated with the same siR-
776 NAs. (**C**) Representative IFM images of serum-deprived RPE1 WT and *CEP78* KO cells treated
777 with control (siMock) or CP110-specific siRNA (siCP110) and stained for ARL13B (green). DAPI

778 marks the nucleus. Dashed boxes indicate cropped images to highlight the centrosomal/ciliary zone.
779 Scale bars, 5 μm in representative images and 1μm in insets. (**D**, **E**) Quantification of percentage of
780 ciliated cells (**D**) and length of remaining cilia (**E**) in RPE1 WT or *CEP78* KO cells treated with
781 control (siMock) or CP110-specific siRNA (siCP110). The quantification is based on images as
782 shown in (C) and represents data from three and four independent experiments, respectively, for
783 RPE1 WT (n=432-455 cells per condition) and *CEP78* KO cells (n=722-846 cells per condition).
784 Ordinary one-way ANOVA with Dunnett's multiple comparison test was used, where RPE1 WT
785 treated with siMock was selected as the control group. a.u., arbitrary units; (*) $p<0.005$; (***)
786 $p<0.001$; (****) $p<0.001$.
787
788

789 **References**

790

791 1. Anvarian, Z., K. Mykytyn, S. Mukhopadhyay, L.B. Pedersen, and S.T. Christensen, *Cellular*
792 *signalling by primary cilia in development, organ function and disease.* Nat Rev Nephrol,
793 2019. **15**(4): p. 199-219.
794 2. Nachury, M.V. and D.U. Mick, *Establishing and regulating the composition of cilia for*
795 *signal transduction.* Nat Rev Mol Cell Biol, 2019. **20**(7): p. 389-405.
796 3. Reiter, J.F. and M.R. Leroux, *Genes and molecular pathways underpinning ciliopathies.* Nat
797 Rev Mol Cell Biol, 2017. **18**(9): p. 533-547.
798 4. Breslow, D.K. and A.J. Holland, *Mechanism and Regulation of Centriole and Cilium*
799 *Biogenesis.* Annu Rev Biochem, 2019. **88**: p. 691-724.
800 5. Spektor, A., W.Y. Tsang, D. Khoo, and B.D. Dynlacht, *Cep97 and CP110 suppress a cilia*
801 *assembly program.* Cell, 2007. **130**(4): p. 678-90.
802 6. Chen, Z., V.B. Indjeian, M. McManus, L. Wang, and B.D. Dynlacht, *CP110, a cell cycle-*
803 *dependent CDK substrate, regulates centrosome duplication in human cells.* Dev Cell,
804 2002. **3**(3): p. 339-50.
805 7. Kleylein-Sohn, J., J. Westendorf, M. Le Clech, R. Habedanck, Y.D. Stierhof, and E.A.
806 Nigg, *Plk4-induced centriole biogenesis in human cells.* Developmental cell, 2007. **13**(2): p.
807 190-202.
808 8. D'Angiolella, V., V. Donato, S. Vijayakumar, A. Saraf, L. Florens, M.P. Washburn*, et al.*,
809 *SCF(Cyclin F) controls centrosome homeostasis and mitotic fidelity through CP110*
810 *degradation.* Nature, 2010. **466**(7302): p. 138-42.
811 9. Li, J., V. D'Angiolella, E.S. Seeley, S. Kim, T. Kobayashi, W. Fu*, et al.*, *USP33 regulates*
812 *centrosome biogenesis via deubiquitination of the centriolar protein CP110.* Nature, 2013.
813 **495**(7440): p. 255-9.
814 10. Sorokin, S., *Centrioles and the formation of rudimentary cilia by fibroblasts and smooth*
815 *muscle cells.* J Cell Biol, 1962. **15**: p. 363-377.
816 11. Sorokin, S.P., *Reconstructions of centriole formation and ciliogenesis in mammalian lungs.*
817 J Cell Sci, 1968. **3**(2): p. 207-30.
818 12. Shakya, S. and C.J. Westlake, *Recent advances in understanding assembly of the primary*
819 *cilium* F1000 Research, In Press.
820 13. Kobayashi, T., W.Y. Tsang, J. Li, W. Lane, and B.D. Dynlacht, *Centriolar kinesin Kif24*
821 *interacts with CP110 to remodel microtubules and regulate ciliogenesis.* Cell, 2011. **145**(6):
822 p. 914-25.
823 14. Huang, N., D. Zhang, F. Li, P. Chai, S. Wang, J. Teng*, et al.*, *M-Phase Phosphoprotein 9*
824 *regulates ciliogenesis by modulating CP110-CEP97 complex localization at the mother*
825 *centriole.* Nat Commun, 2018. **9**(1): p. 4511.
826 15. Cajanek, L. and E.A. Nigg, *Cep164 triggers ciliogenesis by recruiting Tau tubulin kinase 2*
827 *to the mother centriole.* Proc Natl Acad Sci U S A, 2014. **111**(28): p. E2841-50.
828 16. Oda, T., S. Chiba, T. Nagai, and K. Mizuno, *Binding to Cep164, but not EB1, is essential*
829 *for centriolar localization of TTBK2 and its function in ciliogenesis.* Genes Cells, 2014.
830 **19**(12): p. 927-40.
831 17. Lo, C.H., I.H. Lin, T.T. Yang, Y.C. Huang, B.E. Tanos, P.C. Chou*, et al.*, *Phosphorylation*
832 *of CEP83 by TTBK2 is necessary for cilia initiation.* J Cell Biol, 2019. **218**(10): p. 3489-
833 3505.

834 18. Graser, S., Y.D. Stierhof, S.B. Lavoie, O.S. Gassner, S. Lamla, M. Le Clech, *et al.*, *Cep164,*
835 *a novel centriole appendage protein required for primary cilium formation.* J Cell Biol,
836 2007. **179**(2): p. 321-30.
837 19. Goetz, S.C., K.F. Liem, Jr., and K.V. Anderson, *The spinocerebellar ataxia-associated gene*
838 *Tau tubulin kinase 2 controls the initiation of ciliogenesis.* Cell, 2012. **151**(4): p. 847-58.
839 20. Schmidt, K.N., S. Kuhns, A. Neuner, B. Hub, H. Zentgraf, and G. Pereira, *Cep164 mediates*
840 *vesicular docking to the mother centriole during early steps of ciliogenesis.* J Cell Biol,
841 2012. **199**(7): p. 1083-101.
842 21. Tanos, B.E., H.J. Yang, R. Soni, W.J. Wang, F.P. Macaluso, J.M. Asara, *et al.*, *Centriole*
843 *distal appendages promote membrane docking, leading to cilia initiation.* Genes Dev, 2013.
844 **27**(2): p. 163-8.
845 22. Ye, X., H. Zeng, G. Ning, J.F. Reiter, and A. Liu, *C2cd3 is critical for centriolar distal*
846 *appendage assembly and ciliary vesicle docking in mammals.* Proc Natl Acad Sci U S A,
847 2014. **111**(6): p. 2164-9.
848 23. Kurtulmus, B., C. Yuan, J. Schuy, A. Neuner, S. Hata, G. Kalamakis, *et al.*, *LRRC45*
849 *contributes to early steps of axoneme extension.* J Cell Sci, 2018. **131**(18).
850 24. Kanie, T., K.L. Abbott, N.A. Mooney, E.D. Plowey, J. Demeter, and P.K. Jackson, *The*
851 *CEP19-RABL2 GTPase Complex Binds IFT-B to Initiate Intraflagellar Transport at the*
852 *Ciliary Base.* Dev Cell, 2017. **42**(1): p. 22-36 e12.
853 25. Nishijima, Y., Y. Hagiya, T. Kubo, R. Takei, Y. Katoh, and K. Nakayama, *RABL2 interacts*
854 *with the intraflagellar transport-B complex and CEP19 and participates in ciliary assembly.*
855 Mol Biol Cell, 2017. **28**(12): p. 1652-1666.
856 26. Mojarad, B.A., G.D. Gupta, M. Hasegan, O. Goudiam, R. Basto, A.C. Gingras, *et al.*,
857 *CEP19 cooperates with FOP and CEP350 to drive early steps in the ciliogenesis*
858 *programme.* Open Biol, 2017. **7**(6).
859 27. Hossain, D., Y. Javadi Esfehani, A. Das, and W.Y. Tsang, *Cep78 controls centrosome*
860 *homeostasis by inhibiting EDD-DYRK2-DDB1 VprBP.* EMBO Rep, 2017. **18**(4): p. 632-
861 644.
862 28. Yoshida, S., K. Aoki, K. Fujiwara, T. Nakakura, A. Kawamura, K. Yamada, *et al.*, *The*
863 *novel ciliogenesis regulator DYRK2 governs Hedgehog signaling during mouse*
864 *embryogenesis.* Elife, 2020. **9**.
865 29. Nikopoulos, K., P. Farinelli, B. Giangreco, C. Tsika, B. Royer-Bertrand, M.K. Mbefo, *et al.*,
866 *Mutations in CEP78 Cause Cone-Rod Dystrophy and Hearing Loss Associated with*
867 *Primary-Cilia Defects.* Am J Hum Genet, 2016. **99**(3): p. 770-776.
868 30. Ascari, G., F. Peelman, P. Farinelli, T. Rosseel, N. Lambrechts, K.A. Wunderlich, *et al.*,
869 *Functional characterization of the first missense variant in CEP78, a founder allele*
870 *associated with cone-rod dystrophy, hearing loss, and reduced male fertility.* Hum Mutat,
871 2020. **41**(5): p. 998-1011.
872 31. Namburi, P., R. Ratnapriya, S. Khateb, C.H. Lazar, Y. Kinarty, A. Obolensky, *et al.*, *Bi-*
873 *allelic Truncating Mutations in CEP78, Encoding Centrosomal Protein 78, Cause Cone-*
874 *Rod Degeneration with Sensorineural Hearing Loss.* Am J Hum Genet, 2016. **99**(5): p.
875 1222-1223.
876 32. Fu, Q., M. Xu, X. Chen, X. Sheng, Z. Yuan, Y. Liu, *et al.*, *CEP78 is mutated in a distinct*
877 *type of Usher syndrome.* J Med Genet, 2017. **54**(3): p. 190-195.
878 33. de Castro-Miro, M., R. Tonda, P. Escudero-Ferruz, R. Andres, A. Mayor-Lorenzo, J. Castro,
879 *et al.*, *Novel Candidate Genes and a Wide Spectrum of Structural and Point Mutations*
880 *Responsible for Inherited Retinal Dystrophies Revealed by Exome Sequencing.* PLoS One,
881 2016. **11**(12): p. e0168966.

34. Azimzadeh, J., M.L. Wong, D.M. Downhour, A. Sanchez Alvarado, and W.F. Marshall, *Centrosome loss in the evolution of planarians.* Science, 2012. **335**(6067): p. 461-3.
35. Brunk, K., M. Zhu, F. Barenz, A.S. Kratz, U. Haselmann-Weiss, C. Antony*, et al.*, *Cep78 is a new centriolar protein involved in Plk4-induced centriole overduplication.* J Cell Sci, 2016. **129**(14): p. 2713-8.
36. Knudsen, E.S. and J.Y. Wang, *Dual mechanisms for the inhibition of E2F binding to RB by cyclin-dependent kinase-mediated RB phosphorylation.* Mol Cell Biol, 1997. **17**(10): p. 5771-5783.
37. Yan, X., R. Habedanck, and E.A. Nigg, *A complex of two centrosomal proteins, CAP350 and FOP, cooperates with EB1 in microtubule anchoring.* Mol Biol Cell, 2006. **17**(2): p. 634-644.
38. Wang, L., M. Failler, W. Fu, and B.D. Dynlacht, *A distal centriolar protein network controls organelle maturation and asymmetry.* Nat Commun, 2018. **9**(1): p. 3938.
39. Kim, J., J.E. Lee, S. Heynen-Genel, E. Suyama, K. Ono, K. Lee*, et al.*, *Functional genomic screen for modulators of ciliogenesis and cilium length.* Nature, 2010. **464**(7291): p. 1048-51.
40. Shearer, R.F., K.M. Frikstad, J. McKenna, R.A. McCloy, N. Deng, A. Burgess*, et al.*, *The E3 ubiquitin ligase UBR5 regulates centriolar satellite stability and primary cilia.* Mol Biol Cell, 2018. **29**(13): p. 1542-1554.
41. Tsang, W.Y. and B.D. Dynlacht, *CP110 and its network of partners coordinately regulate cilia assembly.* Cilia, 2013. **2**(1): p. 9.
42. Yadav, S.P., N.K. Sharma, C. Liu, L. Dong, T. Li, and A. Swaroop, *Centrosomal protein CP110 controls maturation of the mother centriole during cilia biogenesis.* Development, 2016. **143**(9): p. 1491-501.
43. Walentek, P., I.K. Quigley, D.I. Sun, U.K. Sajjan, C. Kintner, and R.M. Harland, *Ciliary transcription factors and miRNAs precisely regulate Cp110 levels required for ciliary adhesions and ciliogenesis.* Elife, 2016. **5**.
44. Loukil, A., K. Tormanen, and C. Sutterlin, *The daughter centriole controls ciliogenesis by regulating Neurl-4 localization at the centrosome.* J Cell Biol, 2017. **216**(5): p. 1287-1300.
45. Nagai, T., S. Mukoyama, H. Kagiwada, N. Goshima, and K. Mizuno, *Cullin-3-KCTD10-mediated CEP97 degradation promotes primary cilium formation.* J Cell Sci, 2018. **131**(24).
46. Patzke, S., S. Redick, A. Warsame, C.A. Murga-Zamalloa, H. Khanna, S. Doxsey*, et al.*, *CSPP is a ciliary protein interacting with Nephrocystin 8 and required for cilia formation.* Molecular biology of the cell, 2010. **21**(15): p. 2555-67.
47. Frikstad, K.M., E. Molinari, M. Thoresen, S.A. Ramsbottom, F. Hughes, S.J.F. Letteboer*, et al.*, *A CEP104-CSPP1 Complex Is Required for Formation of Primary Cilia Competent in Hedgehog Signaling.* Cell Rep, 2019. **28**(7): p. 1907-1922 e6.
48. Jiang, K., G. Toedt, S. Montenegro Gouveia, N.E. Davey, S. Hua, B. van der Vaart*, et al.*, *A Proteome-wide screen for mammalian SxIP motif-containing microtubule plus-end tracking proteins.* Curr Biol, 2012. **22**(19): p. 1800-7.
49. Satish Tammana, T.V., D. Tammana, D.R. Diener, and J. Rosenbaum, *Centrosomal protein CEP104 (Chlamydomonas FAP256) moves to the ciliary tip during ciliary assembly.* J Cell Sci, 2013. **126**(Pt 21): p. 5018-29.
50. Eguether, T., M.A. Ermolaeva, Y. Zhao, M.C. Bonnet, A. Jain, M. Pasparakis*, et al.*, *The deubiquitinating enzyme CYLD controls apical docking of basal bodies in ciliated epithelial cells.* Nat Commun, 2014. **5**: p. 4585.

928 51. Wang, L., K. Lee, R. Malonis, I. Sanchez, and B.D. Dynlacht, *Tethering of an E3 ligase by*
929 *PCM1 regulates the abundance of centrosomal KIAA0586/Talpid3 and promotes*
930 *ciliogenesis.* Elife, 2016. **5**.
931 52. Douanne, T., G. Andre-Gregoire, A. Thys, K. Trillet, J. Gavard, and N. Bidere, *CYLD*
932 *Regulates Centriolar Satellites Proteostasis by Counteracting the E3 Ligase MIB1.* Cell
933 Rep, 2019. **27**(6): p. 1657-1665 e4.
934 53. Yi, C., Z. Shen, A. Stemmer-Rachamimov, N. Dawany, S. Troutman, L.C. Showe*, et al.*,
935 *The p130 isoform of angiomotin is required for Yap-mediated hepatic epithelial cell*
936 *proliferation and tumorigenesis.* Sci Signal, 2013. **6**(291): p. ra77.
937 54. Hoppeler-Lebel, A., C. Celati, G. Bellett, M.M. Mogensen, L. Klein-Hitpass, M. Bornens*, et*
938 *al.*, *Centrosomal CAP350 protein stabilises microtubules associated with the Golgi*
939 *complex.* J Cell Sci, 2007. **120**(Pt 18): p. 3299-308.
940 55. Belzile, J.P., G. Duisit, N. Rougeau, J. Mercier, A. Finzi, and E.A. Cohen, *HIV-1 Vpr-*
941 *mediated G2 arrest involves the DDB1-CUL4AVPRBP E3 ubiquitin ligase.* PLoS Pathog,
942 2007. **3**(7): p. e85.
943 56. Cox, J. and M. Mann, *MaxQuant enables high peptide identification rates, individualized*
944 *p.p.b.-range mass accuracies and proteome-wide protein quantification.* Nat Biotechnol,
945 2008. **26**(12): p. 1367-72.
946 57. Schou, K.B., J.B. Mogensen, A. Aleliunaite, S.K. Morthorst, I.R. Veland, S.T. Christensen*,*
947 *et al.*, *Kinesin-3 motor protein KIF13B localizes to centrosomes and primary cilia and*
948 *regulates ciliary length and signaling.* Cilia, 2014. **4**(Suppl 1): p. O3.
949 58. Verdier, P., S.K. Morthorst, and L.B. Pedersen, *Targeting of ASH Domain-Containing*
950 *Proteins to the Centrosome.* Methods Mol Biol, 2016. **1454**: p. 15-33.
951 59. Langmead, B. and S.L. Salzberg, *Fast gapped-read alignment with Bowtie 2.* Nat Methods,
952 2012. **9**(4): p. 357-9.
953 60. Kim, D., G. Pertea, C. Trapnell, H. Pimentel, R. Kelley, and S.L. Salzberg, *TopHat2:*
954 *accurate alignment of transcriptomes in the presence of insertions, deletions and gene*
955 *fusions.* Genome Biol, 2013. **14**(4): p. R36.
956 61. Anders, S., P.T. Pyl, and W. Huber, *HTSeq--a Python framework to work with high-*
957 *throughput sequencing data.* Bioinformatics, 2015. **31**(2): p. 166-9.
958 62. Trapnell, C., B.A. Williams, G. Pertea, A. Mortazavi, G. Kwan, M.J. van Baren*, et al.*,
959 *Transcript assembly and quantification by RNA-Seq reveals unannotated transcripts and*
960 *isoform switching during cell differentiation.* Nat Biotechnol, 2010. **28**(5): p. 511-5.
961 63. Robinson, M.D., D.J. McCarthy, and G.K. Smyth, *edgeR: a Bioconductor package for*
962 *differential expression analysis of digital gene expression data.* Bioinformatics, 2010. **26**(1):
963 p. 139-40.
964 64. Love, M.I., W. Huber, and S. Anders, *Moderated estimation of fold change and dispersion*
965 *for RNA-seq data with DESeq2.* Genome Biol, 2014. **15**(12): p. 550.
966

Figure 1

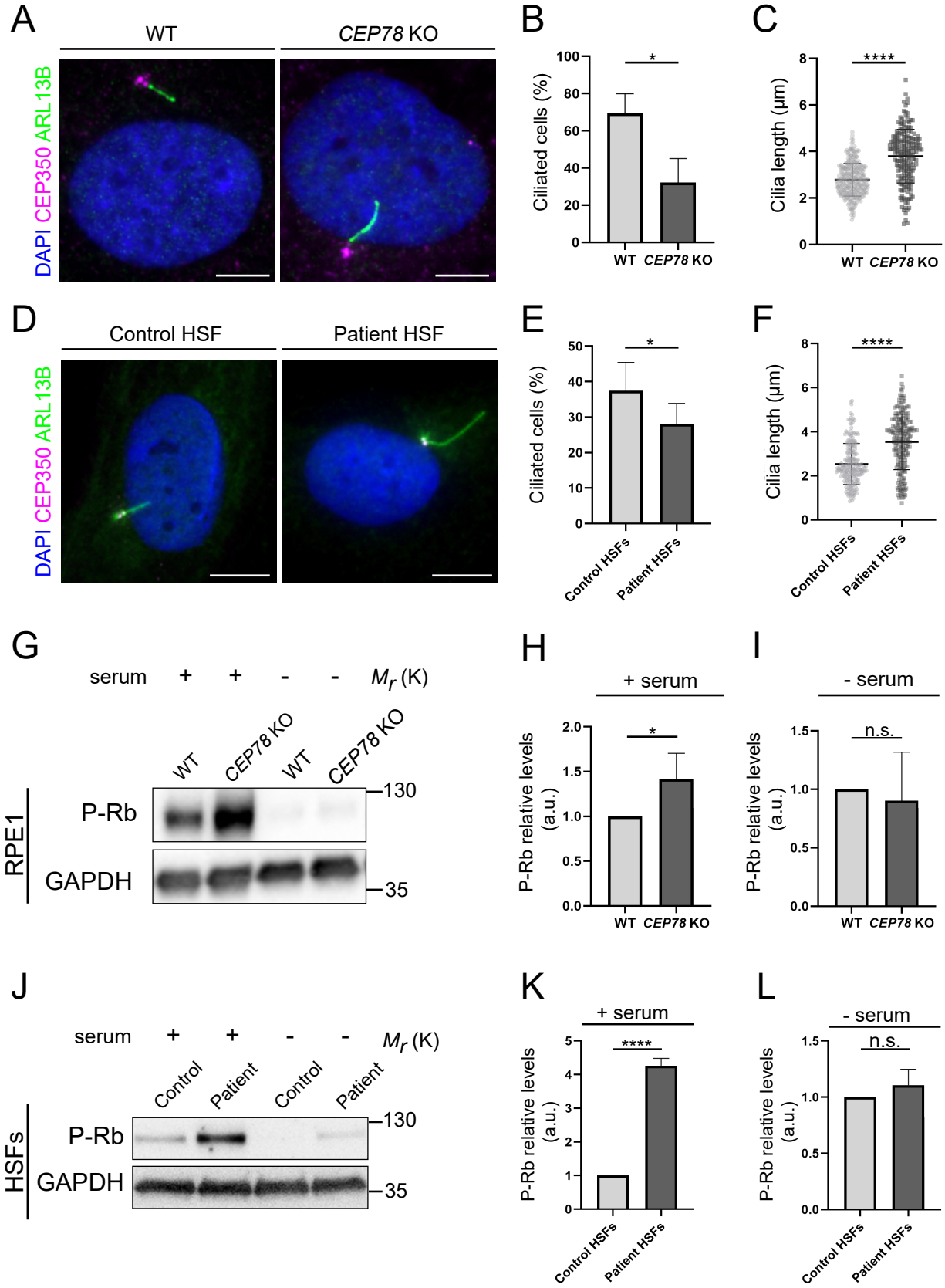
A
WT
CEP78 KO
DAPI CEP350 ARL13B
B
Ciliated cells (%)
*
WT CEP78 KO
C
Cilia length (µm)
****
WT CEP78 KO
D
Control HSF
Patient HSF
DAPI CEP350 ARL13B
E
Ciliated cells (%)
*
Control HSFs
Patient HSFs
F
Cilia length (µm)
****
Control HSFs
Patient HSFs
G
serum + + - - Mr (K)
WT CEP78 KO WT CEP78 KO
RPE1
P-Rb
GAPDH
130
35
H
+ serum
P-Rb relative levels (a.u.)
*
WT CEP78 KO
I
- serum
P-Rb relative levels (a.u.)
n.s.
WT CEP78 KO
J
serum + + - - Mr (K)
Control Patient Control Patient
HSFs
P-Rb
GAPDH
130
35
K
+ serum
P-Rb relative levels (a.u.)
****
Control HSFs
Patient HSFs
L
- serum
P-Rb relative levels (a.u.)
n.s.
Control HSFs
Patient HSFs

Figure 2

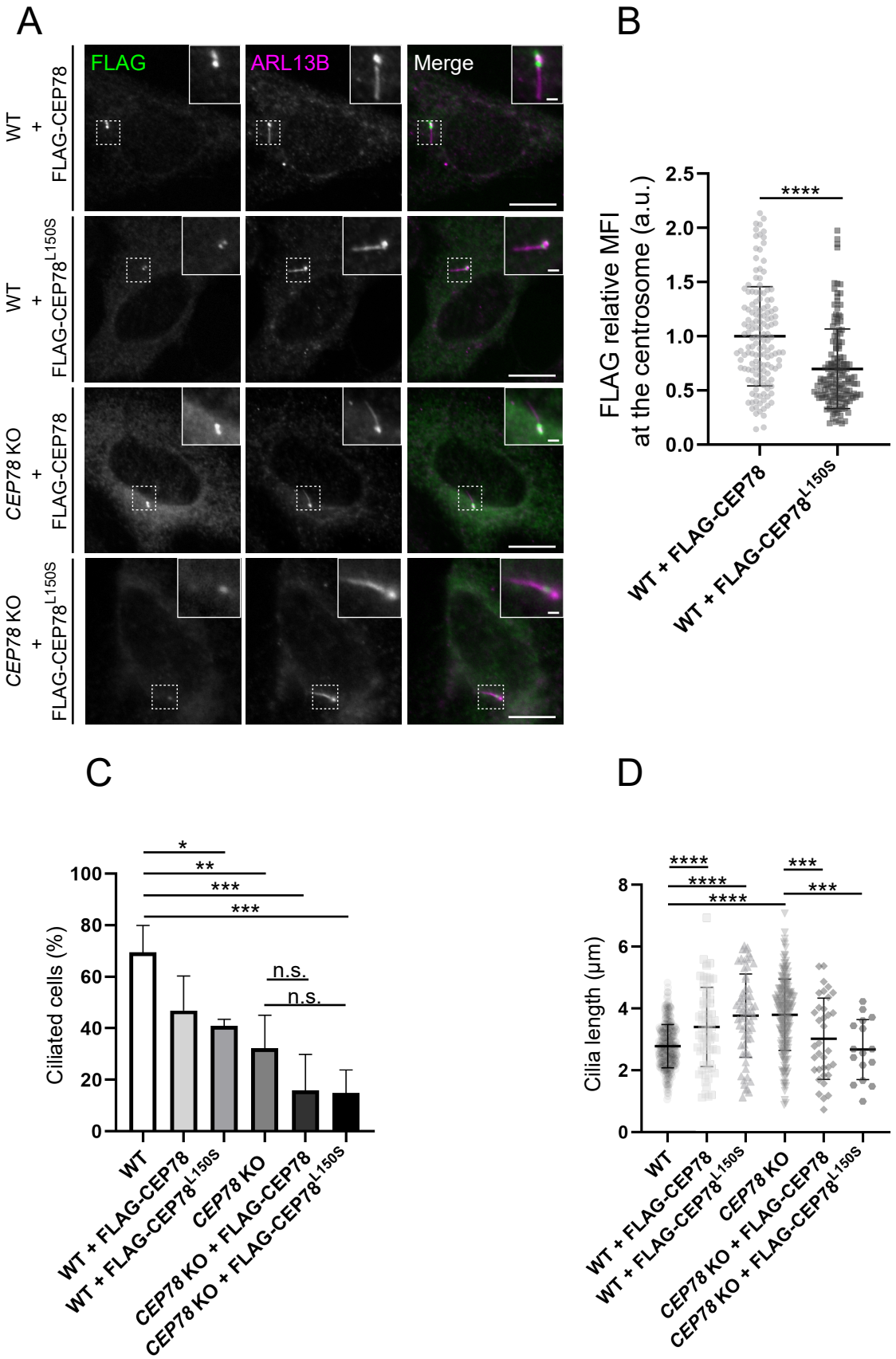
A
FLAG
ARL13B
Merge
WT + FLAG-CEP78
WT + FLAG-CEP78L150S
CEP78 KO + FLAG-CEP78
CEP78 KO + FLAG-CEP78L150S
B
FLAG relative MFI at the centrosome (a.u.)
****
WT + FLAG-CEP78
WT + FLAG-CEP78L150S
C
Ciliated cells (%)
*
**
***
***
n.s.
n.s.
WT
WT + FLAG-CEP78
WT + FLAG-CEP78L150S
CEP78 KO
CEP78 KO + FLAG-CEP78
CEP78 KO + FLAG-CEP78L150S
D
Cilia length (µm)
****
****
****
***
***

Figure 3

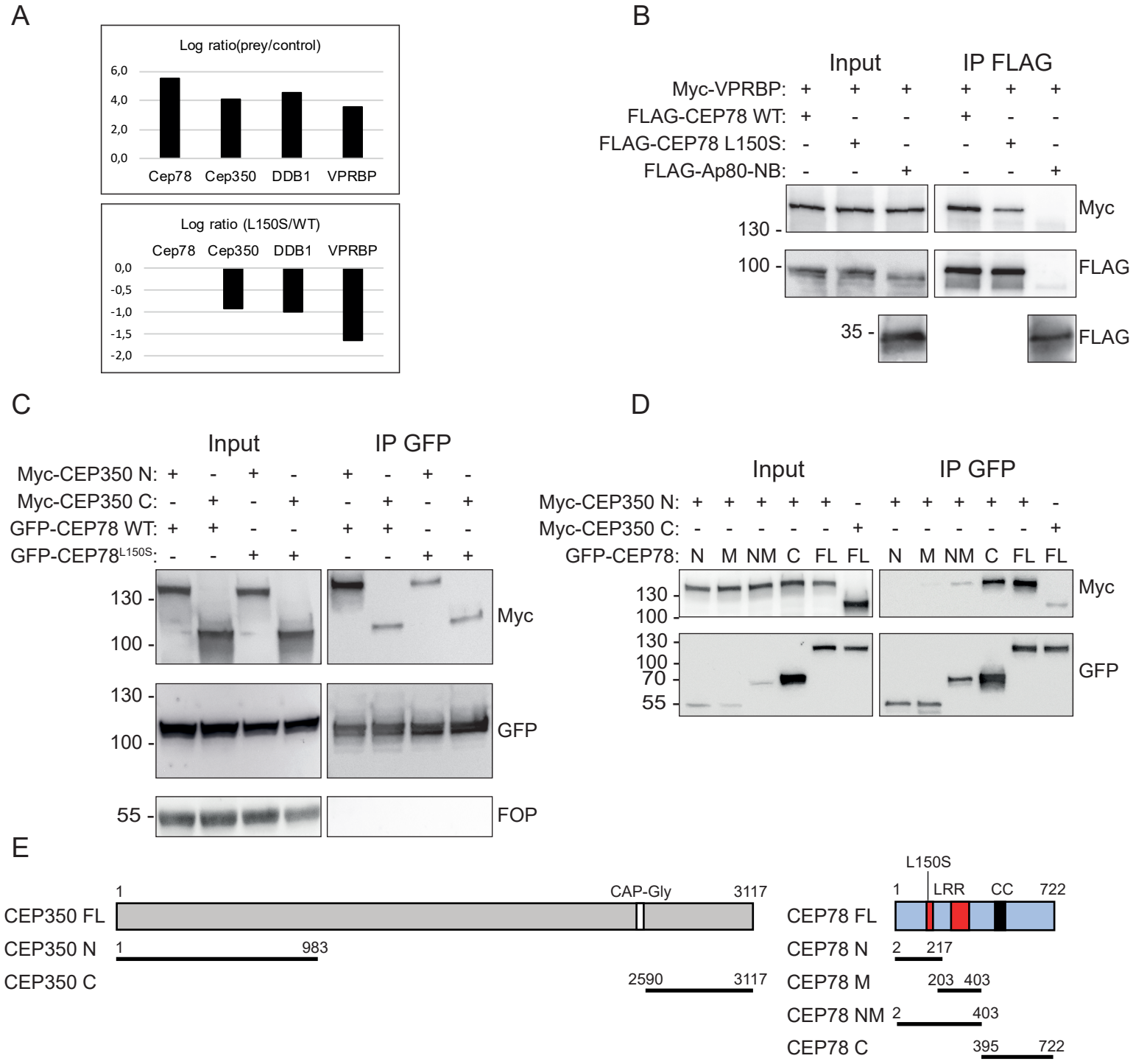
A
Log ratio(prey/control)
6,0
4,0
2,0
0,0
Cep78
Cep350
DDB1
VPRBP
Log ratio (L150S/WT)
Cep78
Cep350
DDB1
VPRBP
0,0
-0,5
-1,0
-1,5
-2,0
B
Input
IP FLAG
Myc-VPRBP: + + + + + +
FLAG-CEP78 WT: + - - + - -
FLAG-CEP78 L150S: - + - - + -
FLAG-Ap80-NB: - - + - - +
130 -
100 -
35 -
Myc
FLAG
FLAG
C
Input
IP GFP
Myc-CEP350 N: + - + - + - + -
Myc-CEP350 C: - + - + - + - +
GFP-CEP78 WT: + + - - + + - -
GFP-CEP78L150S: - - + + - - + +
130 -
100 -
Myc
130 -
100 -
GFP
55 -
FOP
D
Input
IP GFP
Myc-CEP350 N: + + + + + - + + + + + -
Myc-CEP350 C: - - - - - + - - - - - +
GFP-CEP78: N M NM C FL FL N M NM C FL FL
130 -
100 -
Myc
130 -
100 -
70 -
55 -
GFP
E
CEP350 FL
1
CAP-Gly
3117
CEP350 N
1
983
CEP350 C
2590
3117
L150S
1
LRR
CC
722
CEP78 FL
CEP78 N
2
217
CEP78 M
203
403
CEP78 NM
2
403
CEP78 C
395
722

Figure 4

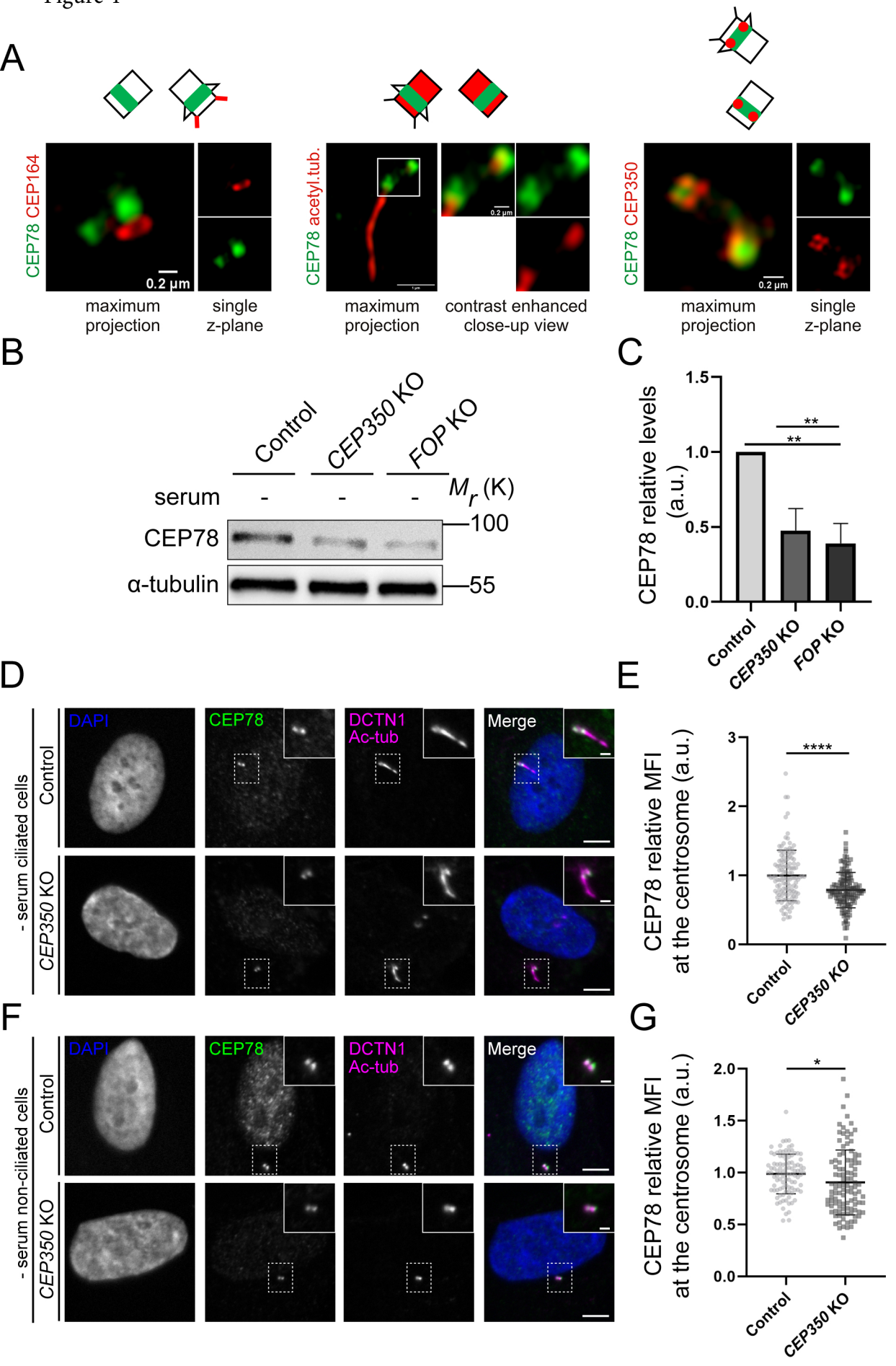
A
CEP78 CEP164
0.2 µm
maximum projection
single z-plane
CEP78 acetyl.tub.
0.2 µm
maximum projection
contrast enhanced close-up view
CEP78 CEP350
0.2 µm
maximum projection
single z-plane
B
Control
CEP350 KO
FOP KO
serum
-
-
-
M_r (K)
CEP78
100
α-tubulin
55
C
CEP78 relative levels (a.u.)
1.5
1.0
0.5
0.0
**
**
Control
CEP350 KO
FOP KO
D
- serum ciliated cells
Control
CEP350 KO
DAPI
CEP78
DCTN1
Ac-tub
Merge
E
CEP78 relative MFI at the centrosome (a.u.)
3
2
1
0
****
Control
CEP350 KO
F
- serum non-ciliated cells
Control
CEP350 KO
DAPI
CEP78
DCTN1
Ac-tub
Merge
G
CEP78 relative MFI at the centrosome (a.u.)
2.0
1.5
1.0
0.5
0.0
*
Control
CEP350 KO

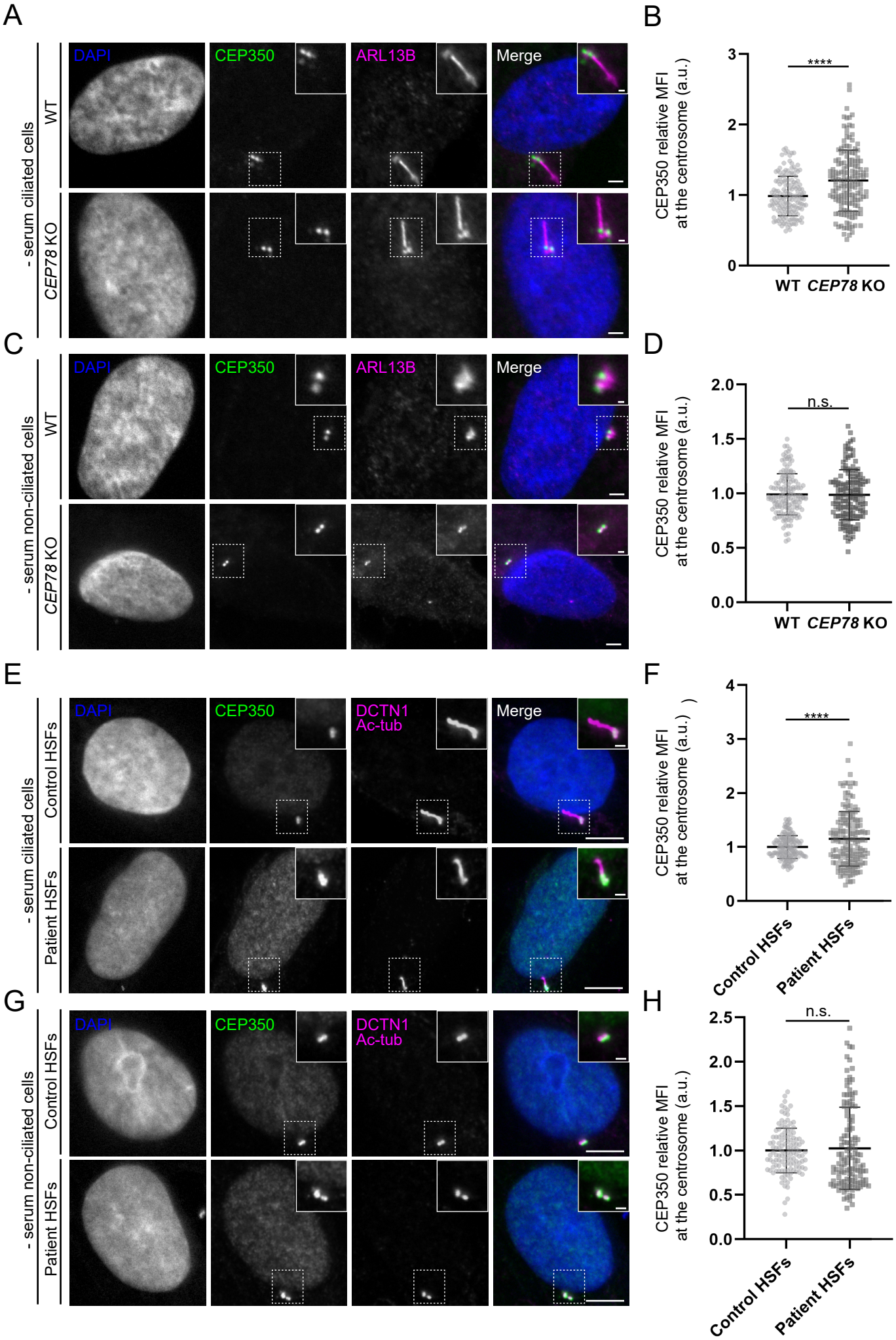
A
- serum ciliated cells
WT
CEP78 KO
DAPI
CEP350
ARL13B
Merge
B
CEP350 relative MFI at the centrosome (a.u.)
****
WT
CEP78 KO
C
- serum non-ciliated cells
D
n.s.
E
Control HSFs
Patient HSFs
DCTN1
Ac-tub
F
G
H

Figure 5

Figure 6

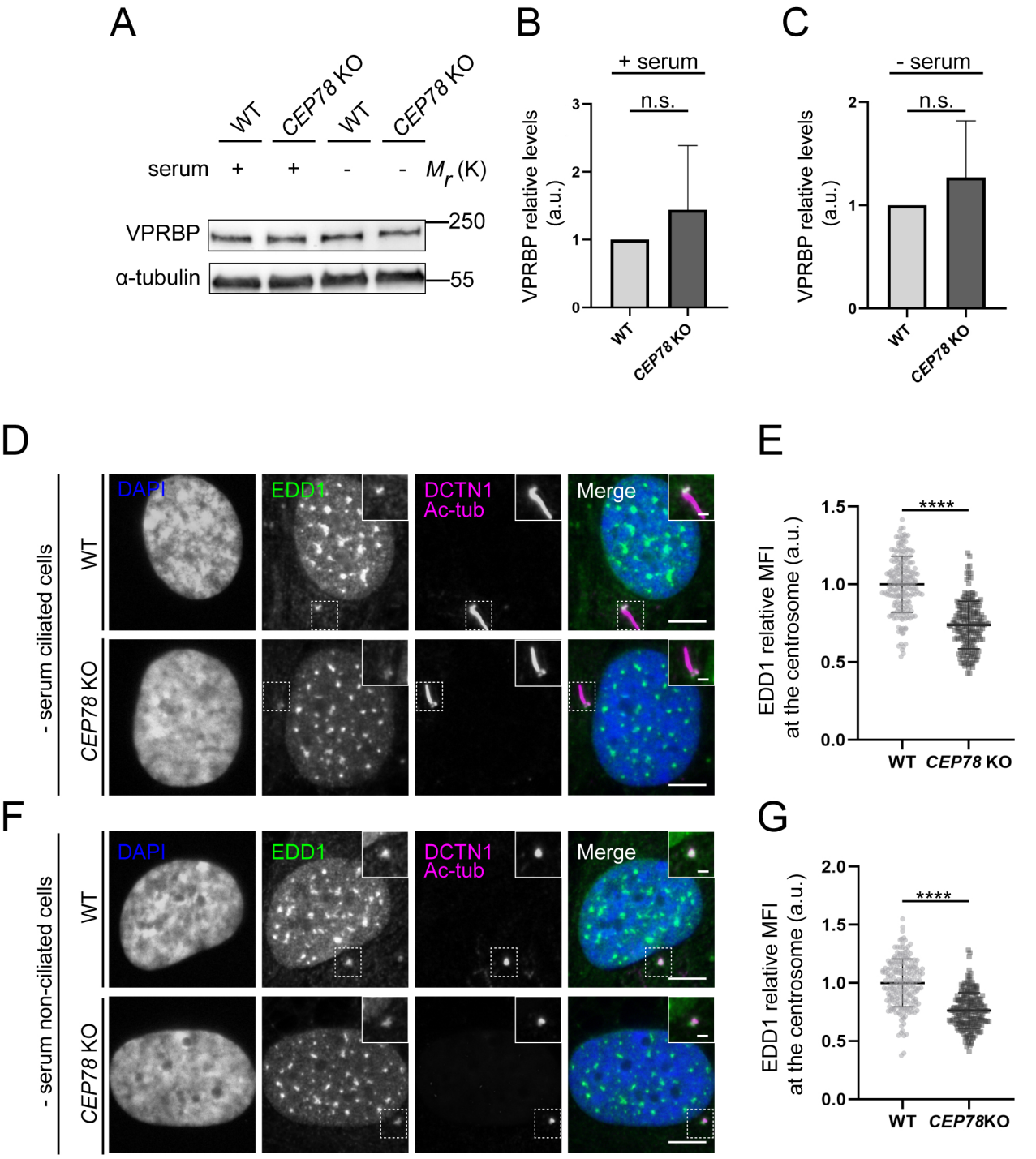
A
WT
CEP78 KO
WT
CEP78 KO
serum + + - - M_r (K)
VPRBP
α-tubulin
250
55
B
+ serum
n.s.
VPRBP relative levels (a.u.)
WT
CEP78 KO
C
- serum
n.s.
VPRBP relative levels (a.u.)
WT
CEP78 KO
D
- serum ciliated cells
WT
CEP78 KO
DAPI
EDD1
DCTN1
Ac-tub
Merge
E
EDD1 relative MFI at the centrosome (a.u.)
****
WT
CEP78 KO
F
- serum non-ciliated cells
WT
CEP78 KO
DAPI
EDD1
DCTN1
Ac-tub
Merge
G
EDD1 relative MFI at the centrosome (a.u.)
****
WT
CEP78KO

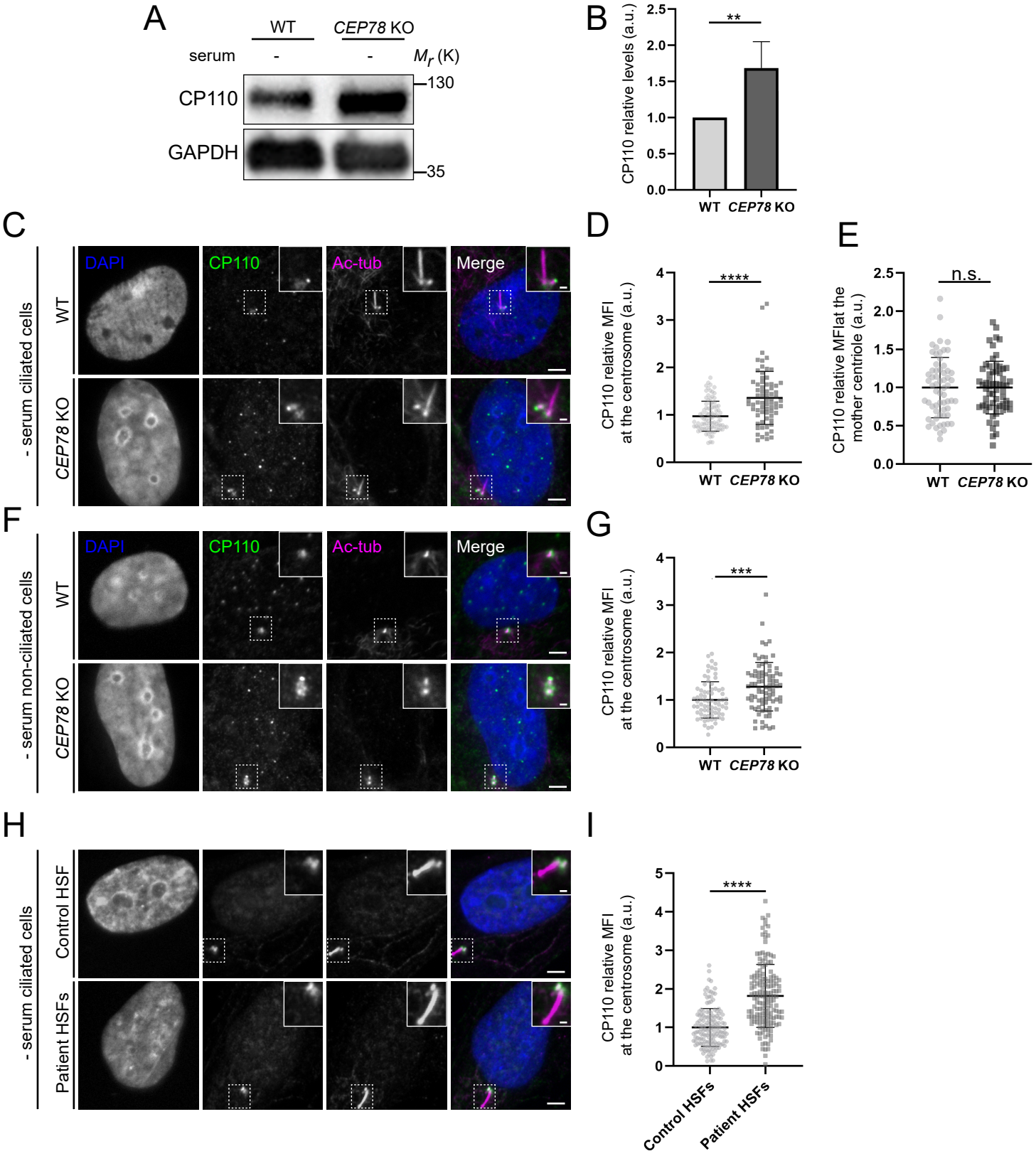
A
WT
CEP78 KO
serum
-
-
Mr (K)
CP110
GAPDH
130
35
B
CP110 relative levels (a.u.)
**
WT
CEP78 KO
C
- serum ciliated cells
WT
CEP78 KO
DAPI
CP110
Ac-tub
Merge
D
CP110 relative MFI at the centrosome (a.u.)
****
WT
CEP78 KO
E
CP110 relative MFIat the mother centriole (a.u.)
n.s.
WT
CEP78 KO
F
- serum non-ciliated cells
WT
CEP78 KO
DAPI
CP110
Ac-tub
Merge
G
CP110 relative MFI at the centrosome (a.u.)
***
WT
CEP78 KO
H
- serum ciliated cells
Control HSF
Patient HSFs
I
CP110 relative MFI at the centrosome (a.u.)
****
Control HSFs
Patient HSFs

Figure 7

Figure 8

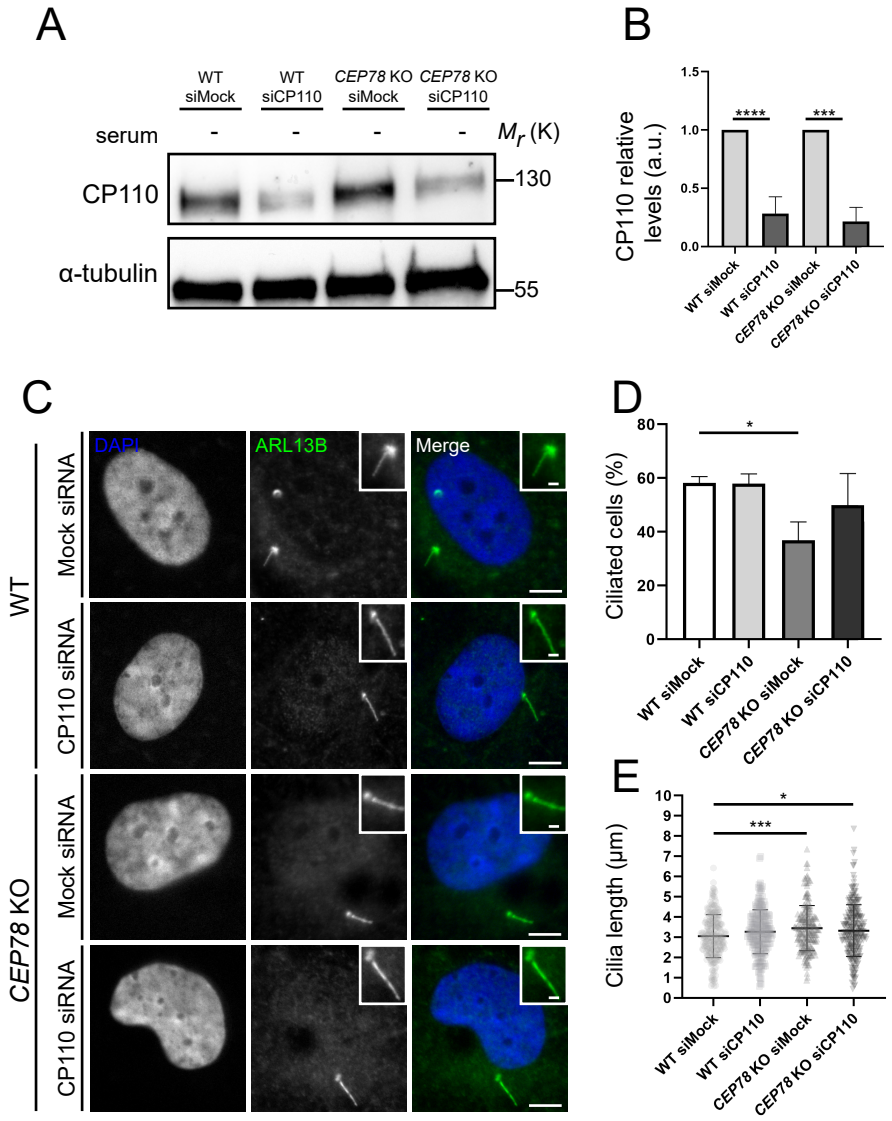
A
WT siMock
WT siCP110
CEP78 KO siMock
CEP78 KO siCP110
serum
Mr (K)
CP110
130
α-tubulin
55
B
CP110 relative levels (a.u.)
****
***
WT siMock
WT siCP110
CEP78 KO siMock
CEP78 KO siCP110
C
WT
CEP78 KO
Mock siRNA
CP110 siRNA
DAPI
ARL13B
Merge
D
Ciliated cells (%)
*
E
Cilia length (µm)
*
***